Journal of Natural Resources and Environmental Management
https://doi.org/10.29244/jpsl.16.2.136

RESEARCH ARTICLE

OPEN ACCESS

Check for updates

Mangrove Distribution, Carbon Stock, and CO_2 Sequestration Mapping Using Sentinel-2 and Field Allometry in Northern Subang, Indonesia

Nyoto Santoso[a,b,c], Rahmat Asy'Ari[c,d], Aulia Ulfa[d], Adam Rachmatullah[a], Oktovianus[e], Yusuf Ramadhan[f]

[a] Department of Forest Resources Conservation and Ecotourism, Faculty of Forestry and Environment, IPB University, IPB Dramaga Campus, Bogor, 16680, Indonesia
[b] Mangrove Study Center of Indonesia, Bogor, 16680, Indonesia
[c] Research Center of Biodiversity and Tropical Forest Rehabilitation (BIOREF IPB), IPB University, Bogor, 11680, Indonesia
[d] SSRS Institute Indonesia, Bogor Regency, Indonesia
[e] Department of Tourism, Trisakti Institute of Tourism, South Jakarta, 12330, Indonesia
[f] Department of Business and Retail Management, Madyathika Polytechnic, Purbalingga, 53317, Indonesia

Article History
Received 17 January 2026
Revised 19 February 2026
Accepted
20 February 2026

Keywords
mangrove, machine learning, subang, sentinel-2

ABSTRACT

Mangrove ecosystems play a crucial role in climate change mitigation through carbon sequestration; however, increasing anthropogenic pressures threaten their function as carbon sinks in these ecosystems. Along the northern coast of Subang, Indonesia, information on mangrove carbon stocks remains limited, despite its importance for sustainable coastal management. This study assessed mangrove distribution and estimated carbon stocks and CO_2 sequestration potential using Sentinel-2 MultiSpectral Instrument (MSI) remote sensing data. The research was conducted over a period of 5 months, from the middle of June to November 2025. The results showed that mangrove density averaged 8,067 ± 5,332 trees ha^{-1}, dominated by *Avicennia marina* (69%). The estimated carbon stocks reached 183.73 ± 97.04 Mg C ha^{-1}, comprising 130.11 ± 70.36 Mg C ha^{-1} of aboveground carbon and 53.62 ± 26.95 Mg C ha^{-1} of belowground carbon. Across 2,684 ha, the total carbon storage was estimated at 268,577 Mg C, equivalent to a CO_2 sequestration potential of 984,782 Mg CO_2e. The Support Vector Machine (SVM) Linear model achieved the highest prediction accuracy (R^2 = 0.86; RMSE = 0.07; MAE = 0.06). These findings highlight the significant contribution of Subang's mangroves to climate change mitigation and provide essential data to support sustainable coastal management and Indonesia's FOLU Net Sink 2030 target.

Introduction

Mangrove forests are intertidal ecosystems that underpin coastal protection, biodiversity, and local livelihoods. Globally, mangroves occupy a relatively small coastal area but provide outsized ecosystem services, such as reducing shoreline erosion, buffering storm impacts, and sustaining fisheries and ecotourism. Beyond these services, mangroves are increasingly central to climate change mitigation because carbon is stored in woody biomass and transferred to long-lived pools through litter inputs and soil organic matter formation [1–3].

This climate function is commonly discussed within the "blue carbon" framework, which links coastal ecosystem conservation to measurable carbon benefits. However, reported mangrove carbon stocks and CO_2-related benefits vary widely across studies and sites, depending on species composition, stand structure and age, disturbance history, and methodological choices (e.g., allometric models, carbon fraction assumptions, and whether soil carbon is included in the analysis). Such variability means that transferring generalized values without careful contextualization can misrepresent both the mitigation potential and management priorities [4–6].

Corresponding Author: Nyoto Santoso nyotosa@apps.ipb.ac.id Department of Forest Resources Conservation and Ecotourism, Faculty of Forestry and Environment, IPB University, IPB Dramaga Campus, Bogor, Indonesia

Indonesia hosts a substantial proportion of the world's mangroves and therefore plays a decisive role in regional blue-carbon outcomes. Simultaneously, many Indonesian mangrove landscapes face persistent conversion pressures, particularly the expansion of aquaculture ponds, which can shift mangroves from net carbon sinks to net carbon sources by releasing stored carbon and reducing future sequestration capacity [2,5,7].

Although national and regional assessments often report indicative emission factors or average carbon values, these summaries rarely capture local uncertainties and methodological differences. For example, emission estimates associated with mangrove loss can differ markedly due to contrasts in baseline mapping, time windows, biomass equations, and conversion factors, as well as differences in hydrological settings. Therefore, a site-specific approach is needed to quantify carbon stocks using transparent, reproducible steps and provide defensible evidence for local planning, restoration prioritization, and potential carbon-based incentives [5,7].

Methodologically, field plots provide the most direct basis for estimating biomass and carbon; however, they are spatially limited and costly to scale. Remote sensing can bridge this gap by mapping the extent of mangroves and enabling the spatial upscaling of plot-derived carbon estimates. Recent work using multispectral satellites and machine learning has improved the accuracy of mangrove classification and carbon prediction; however, comparable, locally validated, and spatially explicit carbon assessments remain limited for many Indonesian coastal districts, including Subang Regency [8–11].

In Subang Regency, mangroves function as a frontline barrier for coastal communities, and the coastline has experienced notable changes over recent decades, alongside reported mangrove decline. These ecological dynamics intersect with livelihood strategies and land-use decisions, making spatially explicit information on mangrove distribution and carbon stocks particularly important for sustainable coastal management planning. Linking anthropogenic pressures to carbon storage locations helps identify priority zones for protection, rehabilitation, and governance interventions.

Accordingly, this study integrates plot-based allometric estimation with Sentinel-2–derived spectral information and machine learning to assess mangroves on the Northern Coast of Subang Regency, Indonesia. This study had three focused objectives: (1) map current mangrove distribution; (2) estimate mangrove carbon stock by upscaling field-derived total carbon stock (TCS) predictions across mapped mangrove areas; and (3) express the resulting carbon stock as CO_2 sequestration potential (Mg CO_2e) to support coastal management and policy evaluation. These outputs are intended to strengthen evidence-based planning by providing spatial coverage and methodological transparency [8].

Materials and Methods

Study Area

The study area is located along the Northern Coast of Subang Regency, West Java Province, Indonesia, covering a low-lying coastal plain that has been extensively modified by aquaculture ponds and estuarine processes. Geomorphologically, this coast is relatively flat and is shaped by fluvial-marine deposition associated with several river mouths and bays (Blanakan Bay and Ciasem Bay), where mangroves commonly occur along estuarine margins and pond boundaries [12,13]. Sediment and substrate conditions are dominated by fine-grained deposits typical of the North Java estuaries. Previous geological descriptions of the Blanakan and Ciasem coastal systems reported floodplain deposits consisting mainly of silty clay/clay, while estuarine deposits were rich in organic material and clay, and marine deposits were dominated by clay and sand (from fine to coarse) with occasional shell fragments [12]. These substrate characteristics are ecologically relevant because they influence root development, sediment carbon storage potential, and distribution of mangrove species across the intertidal zone.

Coastal hydrology is driven by the interaction between river discharge and tidal forcing. Flood mapping in the downstream Ciasem watershed indicates that tidal inundation can extend into pond-dominated areas and settlements during elevated sea levels, underscoring the strong hydrological connectivity between the estuary, intertidal flats, and adjacent land use [13]. The tidal regime in this area is microtidal, with short-term sea-level fluctuations on the order of decimeters, based on the BMKG maritime tide forecast for Patimban Port [14]. The study was conducted from mid-June to November 2025, spanning the late dry season to the onset of the wet season in western Java. This period was selected to maximize the availability of cloud-minimized optical imagery and reduce seasonal bias in canopy conditions for remote sensing–based mapping.

Because the tidal stage can affect the spectral response of mangrove canopies (through water coverage and exposed mudflats), image acquisition dates were matched with tidal information and quality-controlled through cloud masking, as described in the Remote Sensing Data section [14].

The total coastal analysis domain covered approximately 16,573 ha. The spatial extent and distribution of mangrove cover within this domain were quantified using the Sentinel-2 classification results reported in the Results section, providing a consistent basis for upscaling field-derived carbon estimates to the landscape scale. Figure 1 presents a Landsat composite as a regional basemap to illustrate the broader coastal setting and the land-use mosaic. Landsat composites are useful for producing cloud-reduced, synoptic visual context over large areas; however, all primary mangrove mapping and carbon-related modeling in this study used Sentinel-2 imagery (10 m spatial resolution) to ensure methodological consistency with the remote sensing analyses described below [8,12].

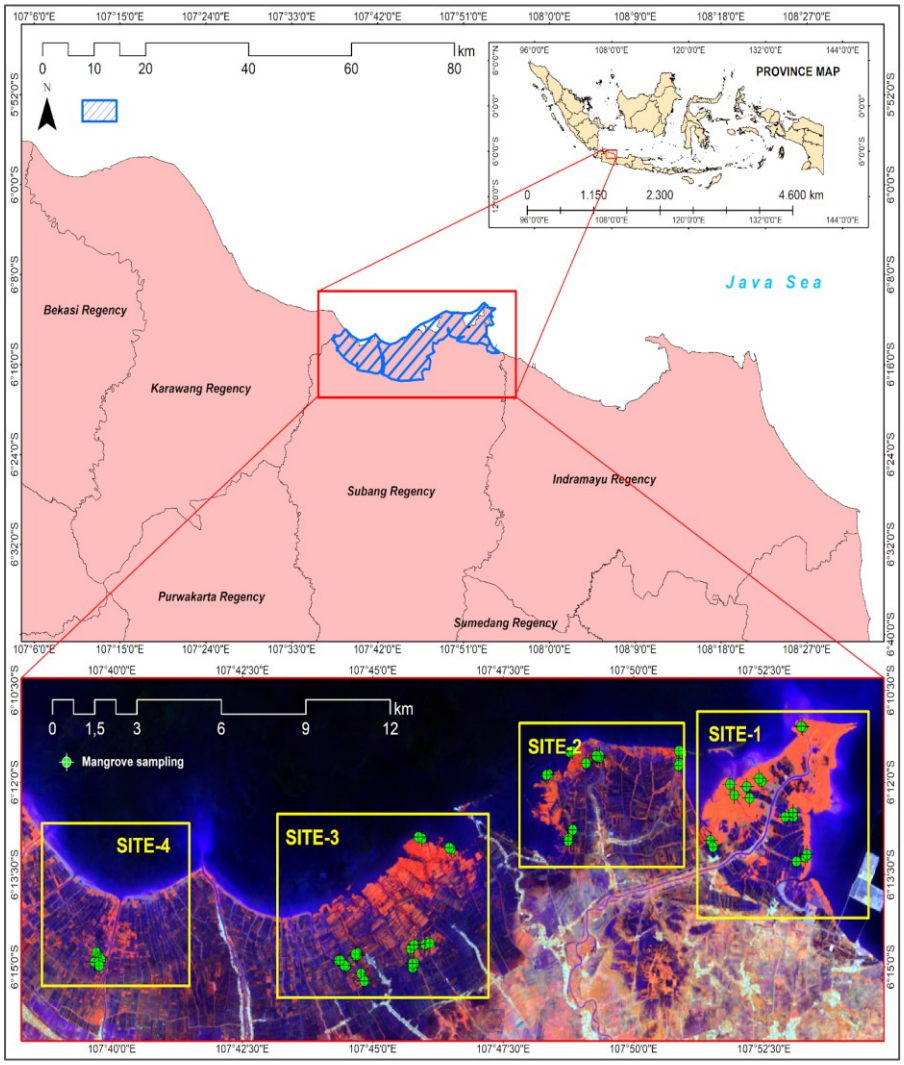

Figure 1. Research location in the northern coastal region of Subang Regency, West Java, Indonesia. This figure presents the geographic location of the study area along the northern coast of Subang Regency using a Landsat composite basemap. The map illustrates the spatial distribution of coastal land uses, including mangrove ecosystems, aquaculture ponds, river estuaries, and surrounding coastal landscapes associated with Blanakan Bay and Ciasem Bay. The study area represents a low-lying coastal plain influenced by fluvial–marine processes and intensive aquaculture development.

Research Design and Flow

This study was conducted through a series of sequential assessments, including the collection of individual mangrove data, calculation of carbon stocks, mapping of mangrove distribution, estimation of carbon stocks, and evaluation of the total carbon stock potential. The overall study workflow is illustrated in Figure 2.

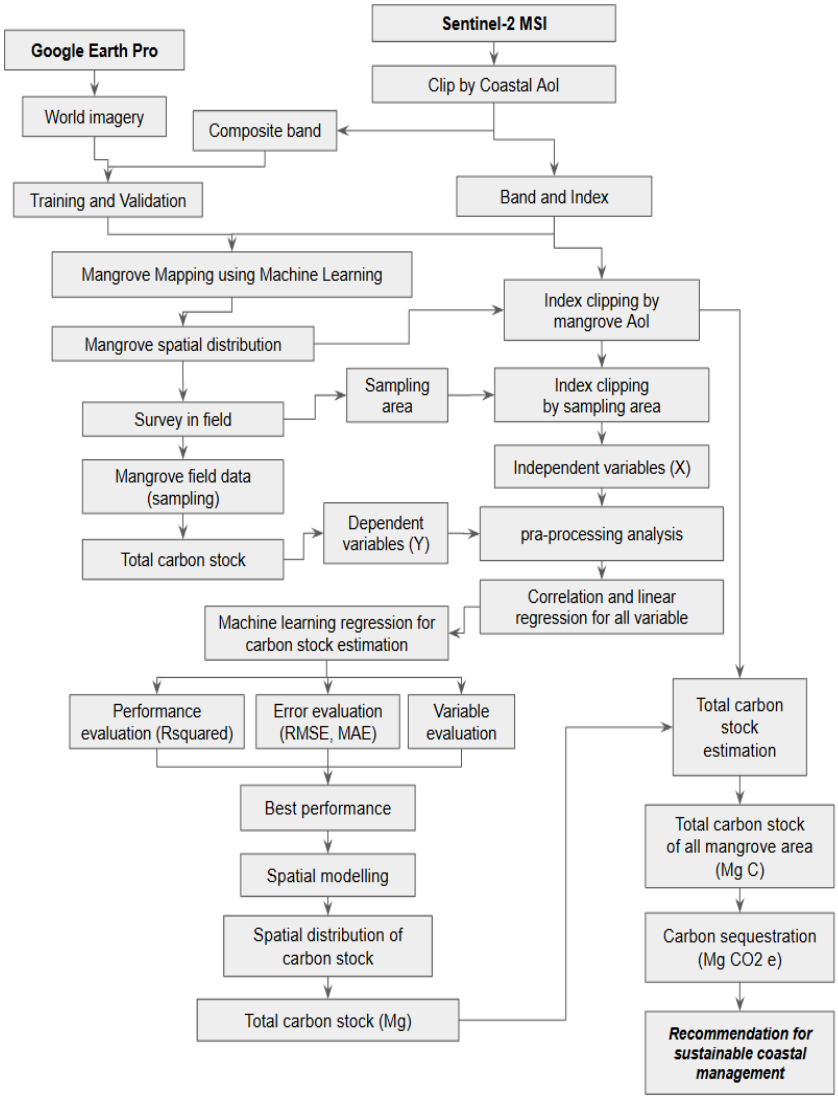

Figure 2. Research flowchart of mangrove assessment and modelling. This figure illustrates the overall methodological framework used to estimate mangrove carbon stocks in the northern coastal region of Subang Regency, Indonesia. The workflow integrates field-based mangrove measurements with Sentinel-2 remote sensing data and spectral indices to develop predictive machine learning models. The resulting model outputs are used to generate spatially explicit estimates of mangrove carbon stock and potential CO_2 sequestration across the study area.

Figure 2 summarizes the methodological workflow of this study. The process begins with field surveys to collect plot-based mangrove attributes (e.g., species identification and DBH measurements). These measurements were converted into plot-level biomass and carbon pools using allometric equations and carbon fraction assumptions, producing plot-level carbon stock values. In parallel, Sentinel-2 MSI imagery was pre-processed (cloud masking and radiometric correction where applicable), and spectral predictors (bands and vegetation indices) were derived for the study period. Field plots were then spatially matched to Sentinel-2 pixels to form the modelling dataset, where plot-level carbon stock served as the response variable and Sentinel-2 predictors served as explanatory variables. A predictive model is trained and evaluated using an explicit validation strategy (e.g., train–test split or cross-validation) and performance metrics (e.g., R^2, RMSE, MAE). The best-performing model was then applied to the Sentinel-2 predictor layers within the mangrove mask to upscale the plot-level values into spatially continuous carbon stock estimates. Finally, carbon stock is reported both as C (Mg C) and as CO_2-equivalent potential using the standard conversion factor (44/12), while uncertainties are discussed in relation to allometric assumptions, plot representativeness, and model prediction errors.

Data Use and Data Sources

Field Data of Mangrove

Mangrove field data were collected through direct surveys along the northern coast of the Subang Regency. To capture spatial heterogeneity, the coastline was divided into four longitudinal sectors (east-west), and sampling points were selected using stratified random sampling based on canopy density classes derived from a preliminary Sentinel-2 NDVI layer. Density strata (low, medium, high, and very high) were defined using natural breaks (Jenks) and verified through reconnaissance. Plot allocation was proportional to stratum area while ensuring that each stratum was represented in every sector to avoid under-sampling sparse or fragmented stands. We also sampled "historical mangroves," defined as areas showing mangrove presence in multi-temporal imagery and/or local land use records but currently degraded, converted, or fragmented, to capture intact and transitional conditions. Site selection combined visual interpretation of high-resolution basemaps to avoid obvious non-mangrove cover and field verification to address commission/omission errors. Where discrepancies occurred, field observations were treated as ground truth, and the labels were corrected accordingly. In total, 59 plots were established across four sites: Site 1-2 each had 16 plots, Site 3 had 21 plots, and Site 4 had six plots, distributed across the four NDVI-based density classes (low, medium, high, and very high).

Mangrove sampling used 10 m × 10 m vegetation plots established within each NDVI density stratum (Figure 3). Within each plot, all trees with DBH ≥ the study threshold were measured for diameter at breast height (DBH) and total height for subsequent carbon stock analyses. DBH was measured at 1.3 m above the ground following standard forestry protocols; for buttressed or irregular stems, the measurement point was adjusted above the deformation and was documented. For multi-stem individuals, each stem was measured and recorded separately. Tree height was measured using a clinometer or laser rangefinder, depending on the field conditions. Species were identified in the field using standard mangrove identification references, supported by photographic documentation of leaves, bark, and propagules, and cross-checked after the survey when necessary. Quality control included instrument calibration at the start of each survey day, repeated measurements for a subset of trees, and consistency checks of plot coordinates (GNSS) to ensure accurate linkage with Sentinel-2 pixels. NDVI-based density strata used for sampling were subsequently evaluated by comparing the field-observed stand structure (e.g., stem density and basal area) across strata to confirm that the classes represented meaningful differences in canopy condition. This verification supports the reliability of the stratification used for both sampling representativeness and subsequent upscaling.

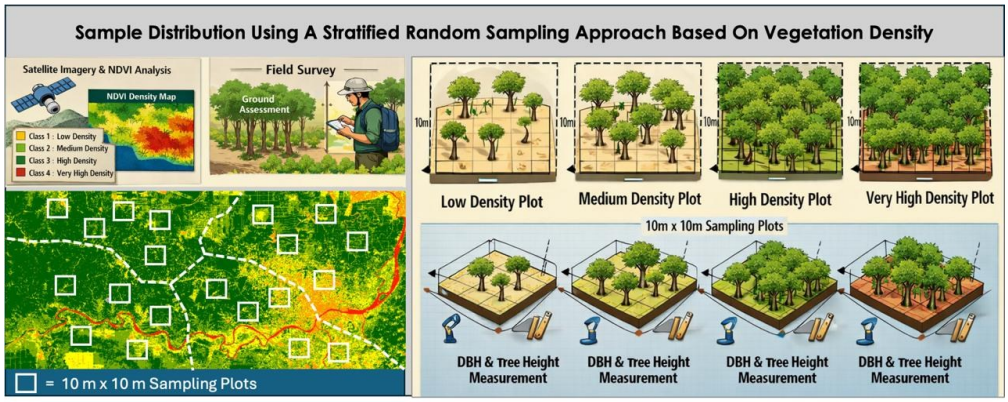

Figure 3. Mangrove sampling design using stratified random sampling based on vegetation density. This figure illustrates the field sampling framework used to collect mangrove structural data along the northern coast of Subang Regency, Indonesia. Sampling plots of 10 m × 10 m were established using a stratified random sampling approach based on NDVI-derived canopy density classes (low, medium, high, and very high) obtained from Sentinel-2 imagery. Within each plot, mangrove attributes including species identification, diameter at breast height (DBH), and tree height were measured to support biomass and carbon stock estimation.

Remote Sensing Data

Sentinel-2 MultiSpectral Instrument (MSI) surface reflectance imagery was used as the primary remote sensing source because its 10 m spatial resolution and 5-day revisit enable detailed mapping of fragmented mangrove patches and frequent revisits needed to mitigate cloud contamination. All imagery was accessed

and processed in Google Earth Engine (GEE) using the collection ee.ImageCollection ('COPERNICUS/S2_SR_HARMONIZED'). The analysis window was set from mid-June to November 2025 to match the field campaign period and maximize the availability of cloud-reduced optical observations during the late dry season to early wet season transition in Java Island, while still capturing representative mangrove canopy conditions.

To derive predictors for classification and regression, we calculated a set of spectral indices representing vegetation vigor, canopy structure, moisture/waterlogging, and built-up influence, which are known to affect mangrove detectability and carbon-related signals in optical data. In total, 14 indices were computed (Table 1). Prior to modelling, we screened the predictors for redundancy and multicollinearity using correlation analysis and variance inflation factors. Highly collinear variables were removed, resulting in 12 indices being retained for model training and spatial prediction. All Sentinel-2 bands and index layers were harmonized to a 10 m resolution to match the finest MSI bands used in the analysis. Index values at field plot locations were extracted from the composite to build the modelling dataset, enabling direct integration between plot-level carbon stock calculations and satellite-derived predictors.

Table 1. Fourteen spectral indices were derived from Sentinel-2 MSI surface reflectance imagery (NIR = near-infrared; SWIR = shortwave infrared) to describe vegetation vigor, canopy structure, moisture/waterlogging, and built-up influence. The table reports each index name, the Sentinel-2 band components used in the calculation, and the corresponding literature source. Indices were computed in Google Earth Engine from mid-June to November 2025 composites over Java Island, Indonesia, and harmonized to 10 m spatial resolution. Collectively, these indices provide the predictor set used for mangrove mapping and carbon-stock modelling by capturing optical signals that help distinguish fragmented mangrove patches from surrounding land covers.

Index	Band Component	References
Normalized Difference Vegetation Index (NDVI)	Red, NIR	[15]
Atmospherically Resistant Vegetation Index (ARVI)	Blue, Red, NIR	[16]
Soil Adjusted Vegetation Index (SAVI)	Red, NIR	[17]
Difference Vegetation Index (DVI)	Red, NIR	[18]
Enhanced Vegetation Index (EVI)	Blue, Red, NIR	[19]
Green Normalized Difference Vegetation Index (GNDVI)	Green, NIR	[20]
Modified Normalized Difference Vegetation Index (MNDVI)	Red Edge 1, Red Edge 2	[21]
Specific Leaf Area Vegetation Index (SLAVI)	Red, NIR, SWIR2,	[22]
Normalized Difference Chlorophyll Index (NDCI)	Red, Red Edge 1	[23]
Normalized Difference Water Index (NDWI)	Green, NIR	[24]
Modified Normalized Difference Water Index (MNDWI)	Green, SWIR2	[25]
Augmented Normalized Difference Water Index (ANDWI)	Blue, Green, Red, NIR, SWIR1, SWIR2	[26]
Land Surface Water Index (LSWI)	NIR, SWIR1	[27]
Normalized Difference Built-up Index (NDBI)	SWIR1, NIR	[28]

Data Analysis

Mangrove Mapping

Mangrove distribution was mapped using Sentinel-2 MSI imagery in Google Earth Engine (GEE) and classified into two classes (mangrove and non-mangrove) using the Random Forest (RF) algorithm. Training samples were generated as stratified points to maintain class balance and spatial coverage across the northern coast of the Subang Regency. To reduce spatial autocorrelation and optimistic accuracy estimates, the training and validation samples were separated using spatially independent partitions (i.e., samples from different areas were allocated to training and validation). RF was implemented with the number of trees and mtry settings reported in the manuscript; hyperparameters were selected to provide stable out-of-bag (OOB) error and consistent variable importance rankings. The final training set was checked for class balance and representation of canopy density gradients, and the validation set was kept independent of the training set to evaluate generalization performance.

Carbon Stock Analysis

The potential carbon reserves of mangroves were assessed using a plot-based approach to determine the stand biomass. Biomass was estimated separately for above-ground biomass (AGB) and below-ground biomass (BGB), as described in Equations 1 and 2. The AGB and BGB calculations utilized diameter at breast

height (DBH) measurements, allometric equations, and species-specific wood density values (Table 2). DBH data were obtained from vegetation surveys conducted during the ground truthing. Subsequently, the AGB and BGB values were converted to aboveground carbon (AGC) and belowground carbon (BGC) using Equations 3 and 4, respectively, by applying a carbon fraction of 0.47. The sum of AGC and BGC yielded the total carbon stock (TCS) at the plot level (Equation 5), as follows: To scale the carbon stock to the landscape, we predicted TCS (Mg C ha^{-1}) for each mangrove pixel using the trained machine learning regression models and then summed the pixel-level carbon stocks across all pixels classified as mangroves (Equation 6). When multiple models were used, the pixel-level estimates were averaged across the models prior to aggregation. Finally, carbon sequestration was reported as a CO_2-equivalent potential derived from the stored carbon stock by multiplying MCS (Mg C) by the molecular weight ratio of CO_2 to C (44/12), following Shih et al. [29] (Equation 7). This CO_2e value represents the potential amount of atmospheric CO_2 associated with the standing vegetation carbon stock (AGC + BGC) at the time of assessment, rather than the annual sequestration rate.

Table 2. Equation list of mangrove biomass allometric. This table presents species-specific and general allometric equations used to estimate mangrove above-ground biomass (AGB) based on diameter at breast height (DBH) measurements obtained from field surveys. It also includes the corresponding wood density values (ρ) from published references, which were used to support biomass and carbon stock estimation in this study.

Mangrove species	Biomass allometric equation	Wood Density (ρ) (g cm-3)	Sources
Avicennia alba	AGB = 0.235 × D 2.42	0.600	Komiyama et al. [30]; SWAMP Cifor
Avicennia marina	AGB = 0.1848 D 2.3524	0.650	Dharmawan and Siregar [31]; MoF, 2013
Bruguiera cylindrica	General equation (Eq.10)	0.763	MoF, 2013
Ceriops decandra	General equation (Eq.10)	0.600	SWAMP Cifor
Rhizophora stylosa	AGB = 0.1579 D 2.593	0.913	Analuddin et al. [32]; MoF, 2013

Above-Ground Biomass

$$AGB\ (kg) = 0.251 \times \rho \times D\ 2.46 \quad (1)$$

Bellow Ground Biomass

$$BGB\ (kg) = 0.199 \times \rho \times 0.899\ x\ D\ 2.22 \quad (2)$$

Above Ground Carbon

$$AGC\ (Mg\ C\ ha^{-1}) = (AGB \times 0.47) / 1{,}000) \times (10{,}000 / Plot\ Area) \quad (3)$$

Bellow Ground Carbon

$$BGC\ (Mg\ C\ ha^{-1}) = (BGB \times 0.47) / 1{,}000) \times (10{,}000 / Plot\ Area) \quad (4)$$

Total Carbon Stock

$$TCS\ (Mg\ C\ ha^{-1}) = AGC + BGC \quad (5)$$

Mangrove Carbon Stock

$$MCS\ (Mg\ C) = A_{pix} \sum_i^N \left(\frac{1}{K} \sum_{k=1}^K TCS_i^{(k)}\right) \quad (6)$$

A pix = Area of one satellite pixel (1 pixel = 100 m² = 0.01 ha)
N = Total number of pixels classified as mangrove area (ha)
K = Number of machine learning algorithms used (e.g., RF, SVM, CART)

CO_2 Sequestration

$$CO_2\ Sequestration\ (Mg\ CO_2\ eq) = MCS \times \left(\frac{44}{12}\right) \quad (7)$$

Carbon Stock Potential Prediction

The potential mangrove carbon stock was predicted using a remote-sensing approach based on satellite imagery [33]. Ground-truth plot data were incorporated into the prediction model as the dependent variable (Y), whereas satellite-derived indices representing vegetation, soil, and water served as independent variables (X) to predict the carbon content within the ground plots. The independent variable values were derived from the Sentinel-2 spectral bands to calculate indices sensitive to mangrove characteristics, thereby enhancing the accuracy of the carbon stock projections (Table 1). The relationships between independent and dependent variables are illustrated in Figure 4. Carbon stock predictions were performed using machine learning regression approaches, including Random Forest (RF), Support Vector Machine (SVM), and

Classification and Regression Tree (CART) algorithms [33,34]. Machine learning analyses were performed using the *caret* package in R Studio [35].

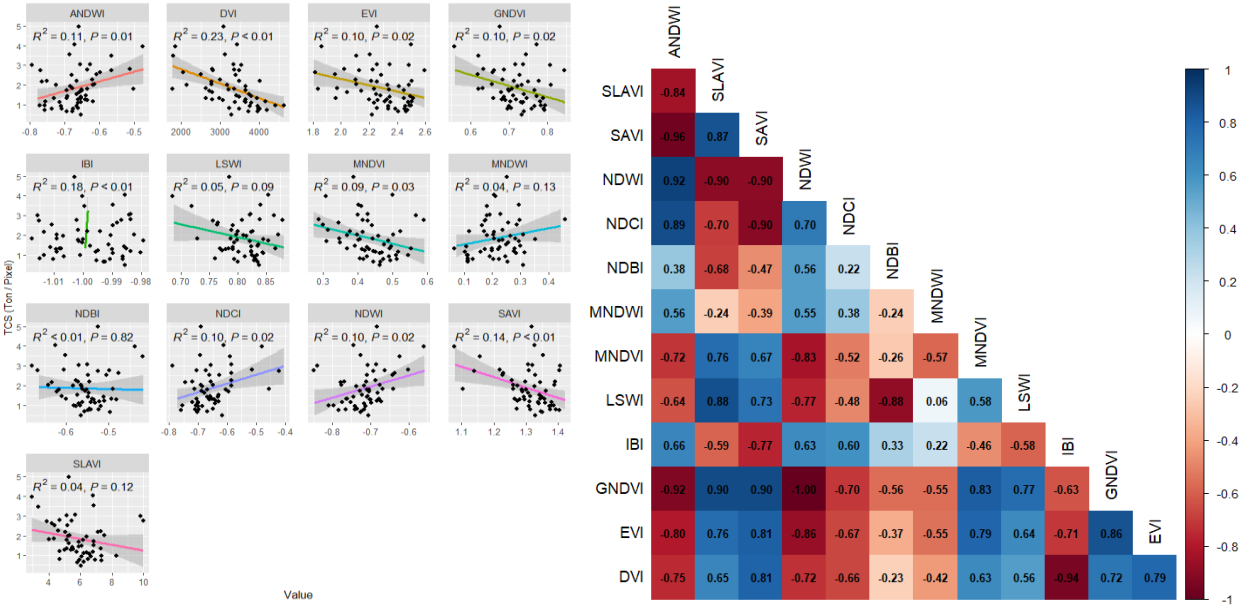

Figure 4. Characteristic of variable independent for carbon stock predicted. The figure presents scatter plots illustrating the relationships between mangrove carbon stock and several Sentinel-2 derived vegetation indices, along with a correlation heatmap among the predictor variables used in the modelling process. These relationships provide an overview of variable behavior and potential multicollinearity among spectral indices prior to their use in machine learning carbon stock prediction.

Performance Evaluation and Error Analysis

The performance of the machine learning-based classification and prediction models was evaluated using variable importance (VI) to quantify the contribution of each predictor. VI assessments were conducted separately for mangrove mapping using the explain function in GEE and for carbon stock prediction models using DALEX: explain in GEE [36]. The model performance and error rates were further evaluated using R-squared (R^2), root mean squared error (RMSE), and mean absolute error (MAE) metrics (Equations 8–10). Additionally, the accuracy of the mangrove mapping models was assessed using overall accuracy (OA) and Kappa statistics (KS) through the error matrix function in GEE (Equations 11 and 12).

$$R^2 = 1 - \frac{\sum_{i=1}^{n}(X_i - Y_i)^2}{\sum_{i=1}^{n}(\underline{Y} - Y_i)^2} \quad (8)$$

$$RMSE = \sqrt{\frac{1}{n}\sum_{i=1}^{n}(X_i - Y_i)^2} \quad (9)$$

$$MAE = \frac{1}{n}\sum_{i=1}^{n}|X_i - Y_i| \quad (10)$$

$$OA = \frac{1}{N}\sum_{i=1}^{r} X_{ii} \times 100\% \quad (11)$$

$$KS = \frac{N\sum_{i=1}^{r} X_{ii} - \sum_{i=1}^{r} X_{ii}(X_{i+} \times X_{+i})}{N^2 - \sum_{i=1}^{r} X_{ii}(X_{i+} \times X_{+i})} \quad (12)$$

Results

Mangrove in Field Side

Overview of Mangrove Condition

Field observations were conducted in 59 plots (0.59 ha; 10 m × 10 m) to represent the canopy density strata and spatial variability along the northern coast. Quantitative metrics (composition, dominance, and

structure) were obtained from plot data, whereas species observed outside the plots were treated as reconnaissance records. Mangroves were mainly associated with river estuaries (particularly the Cipunagara River) and pond embankments/silvofishery settings (Table 3). Stand composition was strongly skewed, *with Avicennia marina* and *Rhizophora stylosa* comprising 69.76% and 29.65% of individuals, respectively (Table 3). This dominance is relevant for carbon accounting because *Avicennia*- and *Rhizophora-dominated* stands can differ in stem form, wood density, and root allocation, affecting allometric biomass estimates and the relative contribution of above- and below-ground carbon.

To make the four field observed distribution patterns reproducible, we defined them using the dominant genus proportion, position along the shore, estuary, pond gradient, and patch configuration relative to land use. Pattern 1: *Avicennia* dominance (>60%) in foreshore/estuarine accretion flats. Pattern 2: Mixed stands (*Avicennia* 30–60%) in silvofishery and pond margins. Pattern 3: *Rhizophora* dominated (>60%) in permanently inundated former ponds and erosion-affected zones. Pattern 4: Linear *Rhizophora* belts along exposed shorelines functioning as wave/current buffers. Figure 5 is a schematic derived from representative transects and GPS-referenced field observations illustrating these criteria (not a pixel-based classification).

Rare species are defined as taxa recorded only off plot or occurring in ≤2 plot records (or <1% of individuals when counts are available). Because key drivers (e.g., tidal range, salinity, and sediment texture) were not measured directly, interpretations related to accretion/erosion/sea level influence or human interventions are presented as plausible mechanisms supported by the observed geomorphic context and discussed conservatively.

Table 3. Information on all collection of mangrove species. The table summarizes the mangrove species identified across the study area, including taxonomic classification, number of individuals recorded within sampling plots, and their relative abundance. Most individuals were dominated by *Avicennia marina* and *Rhizophora stylosa*, while several other species were recorded mainly outside the plots and categorized as reconnaissance or rare observations. The distribution across sampling stations provides an overview of mangrove composition and spatial occurrence along the northern coast of Subang Regency.

No	Species name	Family	Order	Tree individual	% individual	Location
1	*Acanthus ebracteatus*	Acanthaceae	Lamiales	Off-plot	Off-plot	All stations
2	*Acanthus ilicifolius*	Acanthaceae	Lamiales	Off-plot	Off-plot	All stations
3	*Acrosticum speciosum*	Pteridaceae	Polypodiales	Off-plot	Off-plot	St.3
4	*Avicennia alba*	Acanthaceae	Lamiales	14	0.39	All stations
5	*Avicennia marina*	Acanthaceae	Lamiales	2492/2704	69.76	All stations
6	*Barringtonia asiatica*	Lecythidaceae	Ericales	Off-plot	Off-plot	St.3
7	*Bruguiera cylindrica*	Rhizophoraceae	Malpighiales	5	0.14	St.2
8	*Bruguiera gymnorrhiza*	Rhizophoraceae	Malpighiales	Off-plot	Off-plot	St.4
9	*Ceriops decandra*	Rhizophoraceae	Malpighiales	2	0.06	St.2
10	*Clerodendrum inerme*	Lamiaceae	Lamiales	Off-plot	Off-plot	St.1
11	*Derris trifoliata*	Faboideae	Fabaceae	Off-plot	Off-plot	St.1
12	*Excoecaria agallocha*	Euphorbiaceae	Malpighiales	Off-plot	Off-plot	St.3
13	*Rhizophora apiculata*	Rhizophoraceae	Malpighiales	Off-plot	Off-plot	St.1
14	*Rhizophora mucronata*	Rhizophoraceae	Malpighiales	Off-plot	Off-plot	All stations
15	*Rhizophora stylosa*	Rhizophoraceae	Malpighiales	1059/1750	29.65	All stations
16	*Scaevola taccada*	Goodeniaceae	Asterales	Off-plot	Off-plot	St.3
17	*Sonneratia caseolaris*	Lythraceae	Myrtales	Off-plot	Off-plot	St.3
18	*Hibiscus tiliaceus*	Malvaceae	Malvales	Off-plot	Off-plot	St.3

A total of 4,523 mangrove individuals were recorded across 59 sampling plots (0.59 ha). *Avicennia marina* (n = 2,492) and *Rhizophora stylosa* (n = 1,059) dominated the sampled stands, whereas several taxa were detected primarily outside the plots and were treated as locally rare reconnaissance records (for example, *Sonneratia caseolaris* and *Bruguiera* spp.; Table 3). The pattern definitions above provide an interpretive basis for linking field zonation to later carbon estimates, particularly when comparing carbon stocks between *Avicennia-dominated* and *Rhizophora-dominated* plots.

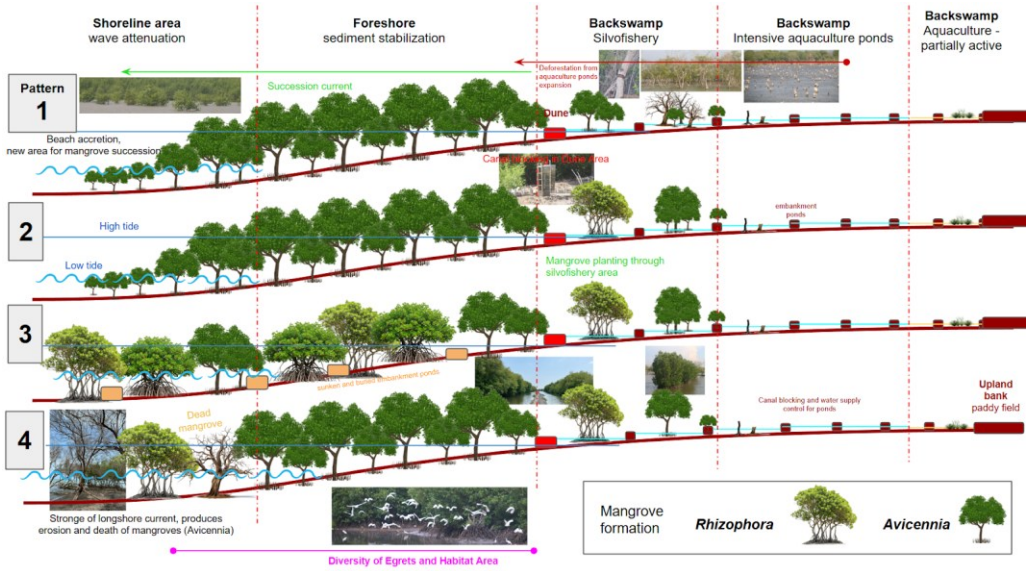

Figure 5. Mangrove zonation pattern in site. The figure illustrates four schematic patterns of mangrove zonation observed along the coastal–inland gradient, ranging from shoreline protection zones to backswamp and aquaculture areas. Each pattern highlights the relative dominance of *Avicennia* and *Rhizophora* formations in relation to geomorphic setting, hydrodynamic exposure, and land-use context. These zonation patterns provide a conceptual framework for interpreting spatial differences in mangrove structure and associated carbon stock distribution across the study sites

Mangrove Biomass, Carbon Stock, and Sequestration

In order to provide a comprehensive understanding of mangrove biomass and carbon stock, it is essential to consider critical variables such as diameter at breast height (DBH), which directly impacts biomass estimations. DBH measurements, obtained during field surveys, were used in conjunction with allometric equations specific to mangrove species to estimate both above-ground and below-ground biomass (AGB and BGB) at the plot level. These estimates are crucial for accurately scaling carbon stocks to landscape levels, especially in the context of heterogeneous mangrove conditions. Table 4 presents detailed mangrove biomass estimations, with variations observed across different sites and species.

Table 4. Mangrove biomass estimations. This table presents the mangrove biomass estimates, including both above-ground biomass (AGB) and below-ground biomass (BGB), from four distinct sites along the northern coast of Subang. The data are categorized by sampling station and mangrove species, showing variations in biomass across different plots and species. The estimates are based on Diameter at Breast Height (DBH) measurements obtained during field surveys and calculated using allometric equations specific to mangrove species. These results highlight the significant spatial variability in carbon stocks, influenced by factors such as stand density, species composition, and environmental conditions.

Sampling	Mean DBH/Plot (cm)	AGB (Kg)	BGB (Kg)
Sampling Station (By Plots)			
Site 1 (16 Plots)	2.83–10.50	239.41–4646.13	125.02–1857.51
Site 2 (16 Plots)	2.80–10.93	1103.02–6137.28	528.87–2479.20
Site 3 (21 (Plots)	2.10–11.05	1642.66–7599.91	764.22–2983.35
Site 4 (6 Plots)	3.36–7.63	707.87–2736.02	333.40–1100.93
Mangrove Species (by Species)			
Avicennia alba	0.95–14.54	0.21–1891.56	0.10–468.32
Avicennia marina	2.83–21.02	73.52–7598.54	33.03–2982.54
Bruguiera cylindrica	1.67–2.87	0.60–16.70.30	0.38–8.37
Ceriops decandra	1.59	1.20	0.77
Rhizophora stylosa	0.64–10.30	0.33–6137.28	0.40–2479.20

The biomass data presented in Table 4 highlight significant spatial variability in mangrove carbon stocks, which are influenced by factors such as stand density, species composition, and environmental conditions across the northern coast of Subang. The observed differences in DBH and biomass between sites, particularly between *Avicennia marina* and *Rhizophora stylosa*, suggest that stand structure plays a pivotal role in carbon accumulation. In this study, DBH was used as a key indicator for estimating the above-ground and below-ground carbon pools, consistent with methods employed in other tropical mangrove forests.

Plot-based estimates showed that above ground carbon (AGC; derived from AGB) ranged from 239.41 to 7,599.91 kg C plot^{-1} (mean 2,772.54 ± 1,509.71 kg C plot^{-1}), while below ground carbon/root biomass (BGC; derived from BGB) reached up to 2,983.35 kg C plot^{-1} (mean 1,134.50 ± 582.60 kg C plot^{-1}) (Figure 6). Because each plot represented 10 m × 10 m (0.01 ha), plot-level carbon (kg C plot^{-1}) was converted to hectare units (Mg C ha^{-1}) by multiplying by 0.1 (1 Mg = 1,000 kg; 1 ha = 100 plots). At the landscape scale, the total mangrove carbon stock was 497,41 Mg C (summed across all mapped mangrove pixels), equivalent to a mean of 183.73 ± 97.04 Mg C ha^{-1} across the mapped mangrove area (2,684 ha) and 1.87 ± 0.97 Mg C per 10 × 10 m pixel/plot.

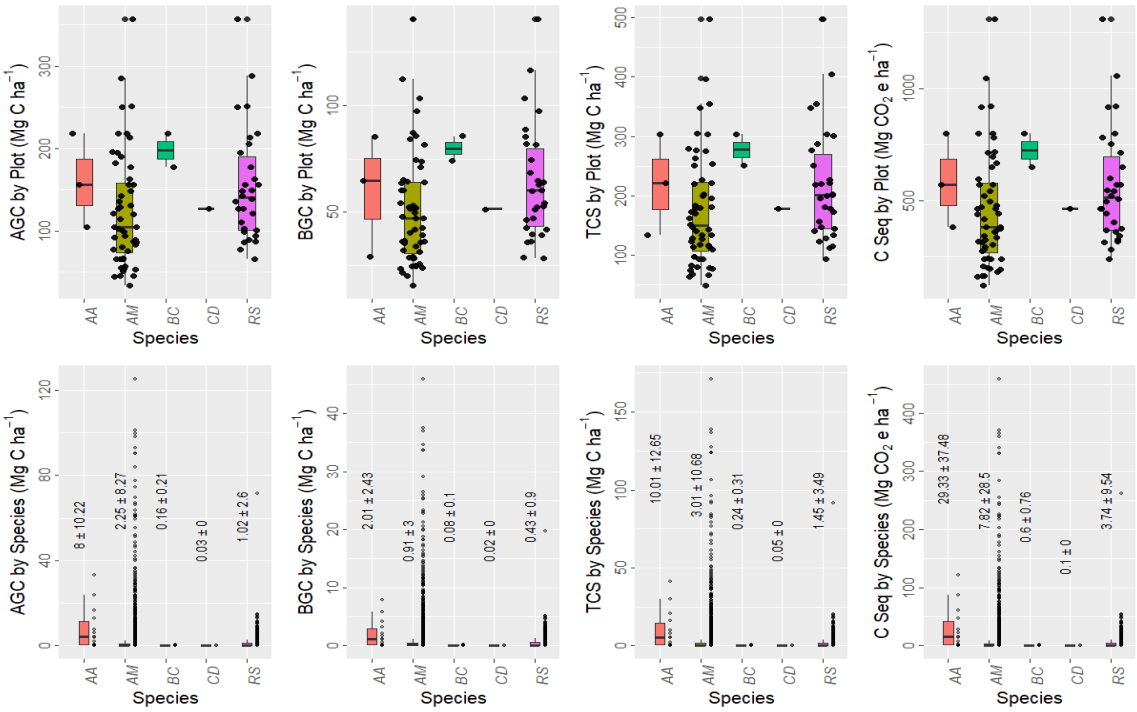

Figure 6. Carbon component in mangrove ecosystem of Northern Coastal of Subang (Note: AA, *Avicennia alba*; AM, *Avicennia marina*; BC, *Bruguiera cylindrica*; CD, *Ceriops decandra*; RS, *Rhizophora stylosa*). This figure illustrates the distribution of carbon components derived from mangrove biomass, including above-ground carbon (AGC) and below-ground carbon (BGC), estimated from field measurements of diameter at breast height (DBH) across sampling plots. The data represent carbon contributions from five mangrove species: *Avicennia alba* (AA), *Avicennia marina* (AM), *Bruguiera cylindrica* (BC), *Ceriops decandra* (CD), and *Rhizophora stylosa* (RS). Carbon values were calculated from biomass estimates obtained in 10 m × 10 m plots distributed across the mangrove ecosystems of the northern coastal area of Subang. The figure highlights substantial variability in carbon stocks among species, with *Avicennia marina* and *Rhizophora stylosa* contributing the largest carbon pools in the studied mangrove stands.

Species-level patterns indicate substantial spatial heterogeneity (large SD), likely reflecting differences in stand structure (DBH distribution, stem density), site history (e.g., rehabilitation vs. remnant stands), and position along estuary–pond–abrasion gradients. *Avicennia marina* exhibited a wide carbon stock range (48.94–497.41 Mg C ha^{-1}) (Figure 6). Plots dominated by *Avicennia* had a TCS of 173.55 ± 98.15 Mg C ha^{-1}, whereas *Rhizophora*-dominated plots averaged 242.35 ± 83.86 Mg C ha^{-1} (Figure 7). Across both stand types, AGC contributed more than BGC; this pattern is consistent with several mangrove carbon studies that have reported higher above-ground contributions in managed or regenerating stands, although the ratios vary by

site and method. Figures 6 and 7 summarize the partitioning of carbon components by species and dominant stand type, highlighting how composition and structure influence total carbon estimates.

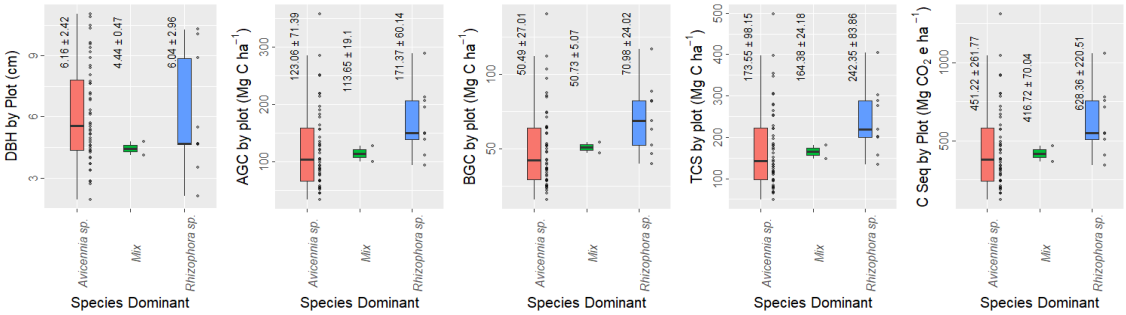

Figure 7. Carbon component in mangrove dominant. This figure compares the distribution of mangrove carbon components between plots dominated by *Avicennia* species and those dominated by *Rhizophora* species. Carbon stocks were estimated from above-ground and below-ground biomass derived from field-measured DBH in 10 m × 10 m sampling plots. The results show that above-ground carbon contributes a larger proportion of total carbon stocks compared with below-ground carbon in both stand types. Overall, *Rhizophora-dominated* stands exhibit higher average total carbon stock than *Avicennia-dominated* stands, indicating differences in stand structure and biomass accumulation between the two mangrove communities.

Mangrove Distribution

Spatial Distribution of Mangrove

Mangrove distribution was mapped from a cloud-minimized Sentinel 2 MSI surface reflectance composite (June–November 2025) using machine learning classification. The resulting mangrove mask delineated 2,684 ha of mangrove along the northern coast of Subang (Figure 8). The map reliability is supported by the independent accuracy assessment reported in Section Mangrove Biomass, Carbon Stock, and Sequestration (150 validation pixels; OA = 84%; KS = 0.77), which provides a quantitative basis for interpreting the spatial patterns. Spatially, mangroves cluster around river estuaries, most prominently in the eastern sector (Site 1), where fluvial inputs and intertidal deposition create suitable substrates, and around pond-dominated landscapes in the central coast (Site 3), including former ponds affected by abrasion and permanent inundation. The map also shows smaller, fragmented patches embedded within silvofishery and pond margin settings, often forming linear belts along embankments and shorelines, consistent with planting and protection. These patterns align with the training scheme that sampled mangrove and non-mangrove classes across estuary margins, aquaculture ponds, mudflats, and built-up areas, and with the high importance of water-related indices (e.g., MNDWI/LSWI) in separating mangroves from surrounding waterlogged surfaces. Because narrow shore belts and pond margins are susceptible to mixed pixels and tidal inundation effects, we interpret fine-scale fragmentation and edge locations conservatively and focus on robust hotspots (estuaries, former ponds, and silvofishery mosaics) that are consistently detected across the composite.

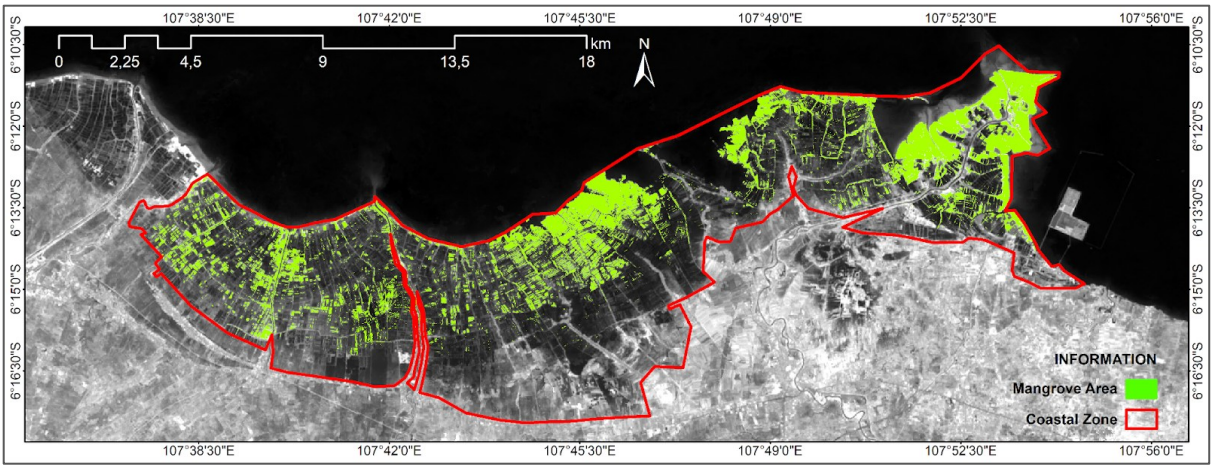

Figure 8. Spatial distribution of result mangrove mapping. The figure presents the spatial extent and distribution of mangrove ecosystems mapped using a machine learning classification of Sentinel-2 MSI surface reflectance composite data for June-November 2025. Mangrove areas are primarily concentrated around river estuaries and pond-dominated coastal landscapes, forming clusters and linear belts along shorelines and aquaculture embankments. The map highlights major mangrove hotspots and fragmented patches, providing a spatial basis for subsequent analysis of mangrove carbon stock and ecosystem condition.

Evaluation of Mangrove Mapping

A total of 150 validation points (pixels) were used to assess the accuracy of the mangrove map produced using the Google Earth Engine (GEE). Validation points were generated independently from the training samples (no overlap) and were distributed across the study area to reduce spatial autocorrelation. Of the 150 points, 23 were misclassified, yielding an overall accuracy (OA) of 84% and a Kappa statistic of 0.77 (Figure 9). To improve interpretability, class-specific producer and user accuracies (and the confusion matrix) are now reported alongside OA and Kappa, and the dominant error modes are summarized in the text.

The variable importance from the tuned Random Forest model indicated that the Modified Normalized Difference Water Index (MNDWI) was the most influential predictor, followed by LSWI, whereas EVI contributed the least (Figure 9). This is consistent with the Subang coastal setting, where mangrove pixels often contain mixed canopy-water signals due to tidal inundation, pond margins, and waterlogged soils; therefore, water indices strengthen the separation from open water, mudflats, and wet bare substrates.

The mean variable importance value (54) was used as a descriptive reference line to highlight above-average contributors rather than as a strict selection rule; accordingly, only four indices (MNDWI, LSWI, NDBI, and SLAVI) exceeded this mean. Potential redundancy among predictors was reduced during preprocessing via correlation screening; therefore, variable importance rankings were interpreted as relative contributions within the screened predictor set. Figure 9 should be interpreted in two parts: the validation output summarizes the agreement and commission/omission errors, whereas the variable importance plot highlights the predictors that most influence class separation. Therefore, we interpret fine-scale fragmentation and narrow shoreline belts conservatively because these areas are most sensitive to mixed pixels and tidal state variability, whereas estuary and pond margin concentrations remain robust at the composite mapping scale.

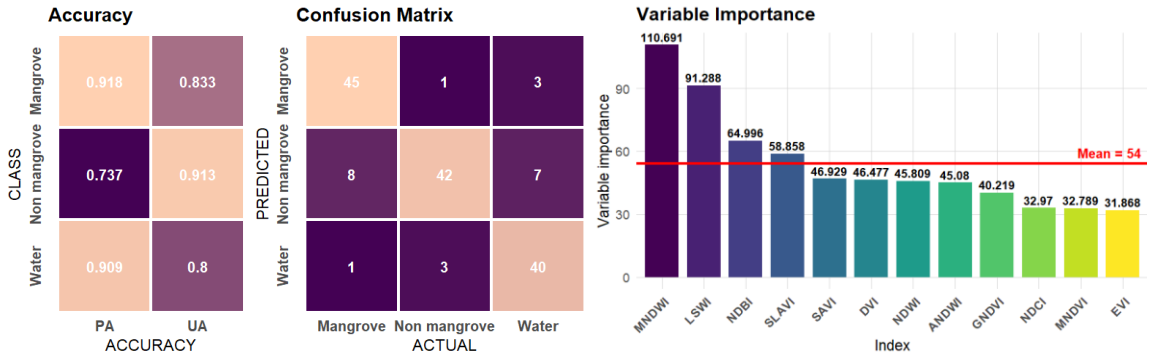

Figure 9. Validation test and variable importance of machine learning performance for mangrove mapping. The figure presents the validation results of the mangrove classification using 150 independent validation pixels, showing the overall accuracy and agreement between predicted and reference classes. It also illustrates the relative importance of spectral indices used in the Random Forest model, highlighting key predictors such as MNDWI and LSWI that contribute most to mangrove discrimination. These results support the reliability of the mapping approach and identify the spectral variables that most influence model performance.

Modelling Result of Total Carbon Stock of Mangrove

Machine Learning Regression for Mangrove Carbon Modelling

Machine learning models effectively predicted the mangrove carbon stocks in the study area. The best performance was achieved using the Support Vector Machine (SVM) algorithm with hyperparameter tuning, particularly the SVM Polynomial model, which yielded an R-squared (R^2) of 0.88, a root mean squared error (RMSE) of 0.065, and a mean absolute error (MAE) of 0.058 (Figure 10). The Random Forest (RF) and Classification and Regression Tree (CART) algorithms produced comparable performance metrics. Across the six models and three algorithms, the average R^2 was 0.97, RMSE was 0.07, and MAE was 0.06. The lowest R^2 was observed in the CART algorithm using the rpart2 model (R^2 = 0.82; RMSE = 0.066). Visual inspection of hyperparameter tuning results indicated that SVM, particularly the SVM Polynomial model, and the CART rpart model exhibited more variable R^2 distributions, with values of 0.84 ± 0.02 (SVM Polynomial), 0.86 ± 0.01 (CART rpart), and 0.87 ± 0.01 (SVM Linear). Similarly, the RMSE and MAE distributions were more variable in the SVM models, notably the SVM Polynomial (RMSE = 0.25 ± 0.19; MAE = 0.20 ± 0.14). Normality tests on the hyperparameter-tuned results indicated that only the RF algorithm produced R^2, RMSE, and MAE values that were normally distributed, with p-values ranging from 0.14 to 0.91.

Machine learning regression models were used to predict plot-derived total carbon stock (TCS) from Sentinel-2 predictors. Model tuning and internal performance screening were conducted on the training data using repeated k-fold cross-validation (k = 10; 5 repeats) to reduce sensitivity to a single split. Accordingly, the values reported with the "±" notation in Figure 10 represent the mean ± standard deviation across cross-validation resamples (i.e., model stability during tuning), rather than a single-point estimate.

Across the tuned candidates, the performance during resampling was broadly comparable (R^2 range: 0.82–0.88). The highest resampling performance was obtained by the SVM Polynomial configuration (mean R^2 = 0.84 ± 0.02; mean RMSE and MAE shown in Figure 10), while RF and CART produced similar mean performance with slightly lower variability. We emphasize that the final model selection and reported predictive performance were based on independent validation results (Figure 12) to avoid data leakage and overly optimistic estimates from tuning-only outputs. Therefore, we removed the previously stated "average R^2 = 0.97" across models, which could be misinterpreted, and we now report performance consistently as cross-validated tuning stability (Figure 10) and independent validation accuracy (Figure 12). Finally, we omitted the normality testing of resampled metrics because normality is not a requirement for model generalization; instead, we interpreted dispersion (SD) as an indicator of stability across resamples.

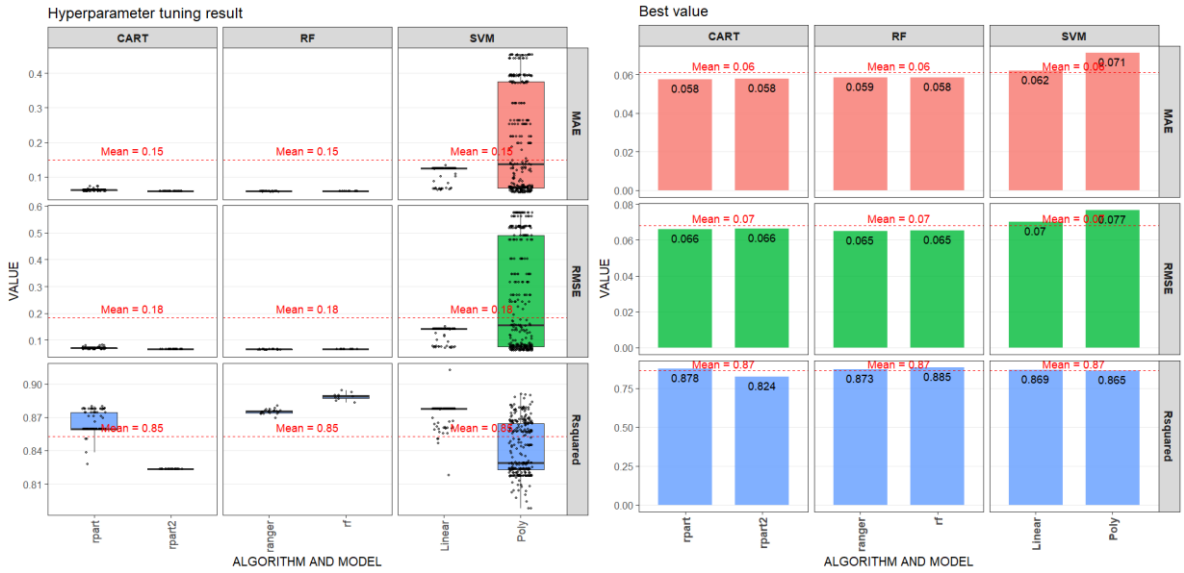

Figure 10. R-squared, RMSE, and MAE from hyperparameter tuning on several algorithms for mangrove carbon stock predicted. The figure presents the distribution of model performance metrics (R^2, RMSE, and MAE) obtained during repeated k-fold cross-validation for several machine learning algorithms used to predict mangrove total carbon stock from Sentinel-2 predictors. The results illustrate the comparative stability and predictive capability of the tested models, highlighting the SVM Polynomial configuration as one of the best-performing candidates during the tuning stage. These metrics represent the mean and variability across resampling iterations, indicating model robustness prior to independent validation.

Predicted Performance Evaluation

To improve interpretability, the model evaluation is presented as a two-stage process linking Figures 10–12. Figure 10 summarizes the hyperparameter tuning performance as mean ± SD across repeated k-fold cross-validation resamples, which is used to assess training stage stability and reduce the overfitting risk. Figure 11 reports the within-algorithm predictor rankings and is interpreted qualitatively within each model (not as a directly comparable score across RF, SVM, and CART). Finally, Figure 12 presents the independent validation performance (single-point R^2, RMSE, and MAE on the held-out dataset), which is the primary basis for comparing the algorithms and selecting the final model. This staged reporting reconciles the differences between tuning statistics and validation outcomes by explicitly stating that the former reflects resampling stability, whereas the latter reflects predictive generalization.

Ecologically, the dominant predictors were consistent with the key controls on mangrove canopy signals in an intertidal landscape. Vegetation indices emphasizing greenness and canopy vigor (e.g., MNDVI/DVI) likely proxy canopy density and structural conditions that co-vary with plot-derived carbon stocks, whereas water/moisture indices (e.g., MNDWI/LSWI/ANDWI) become influential where tidal inundation, pond margins, and waterlogged substrates generate mixed pixels and strong water adjacency effects. Where built-up or edge-related indices contribute (e.g., NDBI), they plausibly capture anthropogenic boundaries and fragmentation that affect stand conditions and spectral mixing. Because uncertainty arises from both field-based carbon estimation (allometry/wood density/measurement) and mapping uncertainty (classification errors and mixed pixels), the predicted carbon surfaces were interpreted conservatively, particularly along narrow shoreline belts and highly fragmented patches.

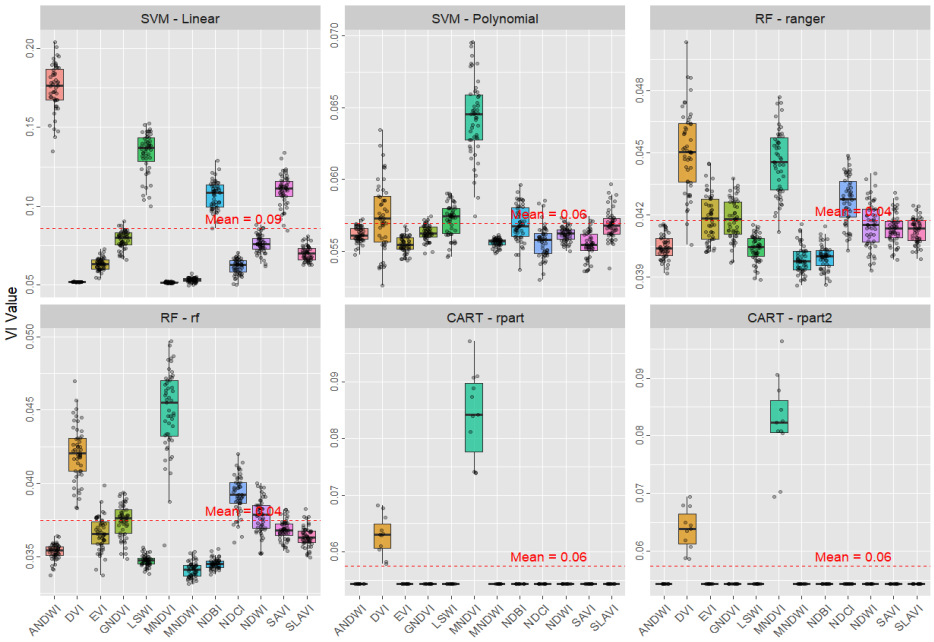

Figure 11. Variable importance of spectral predictors from hyperparameter-tuned machine learning models for mangrove carbon stock prediction. The figure illustrates the relative importance of Sentinel-2–derived spectral indices used as predictors in the machine learning models for estimating mangrove total carbon stock. Variable importance values are presented within each algorithm to indicate the relative contribution of vegetation, water, and land-surface indices to model predictions. These results highlight the predictors that most strongly influence the estimation of mangrove carbon stocks in the intertidal coastal environment.

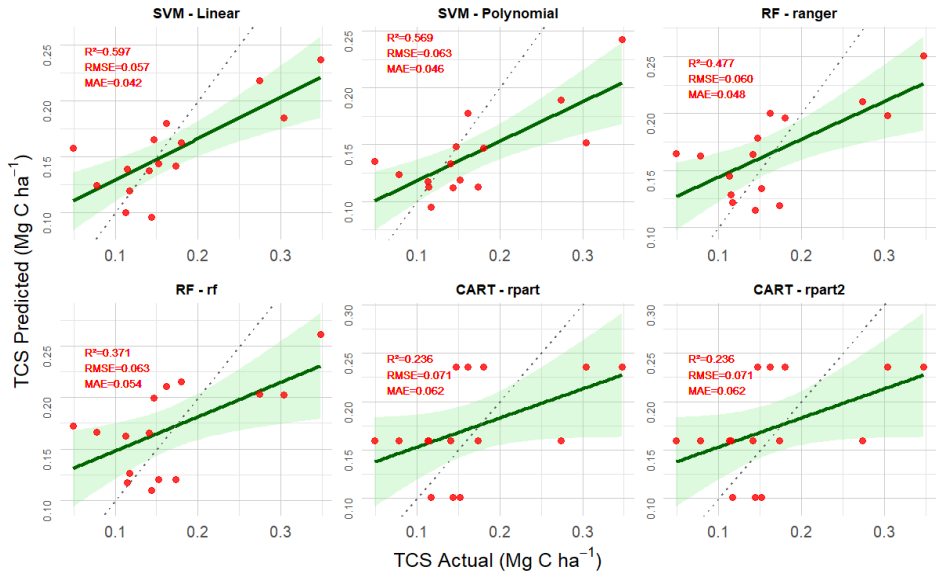

Figure 12. Validation test for machine learning algorithm and model. This figure presents the validation results of three machine learning algorithms—Random Forest (RF), Support Vector Machine (SVM), and Classification and Regression Tree (CART)—for estimating mangrove total carbon stock. Model performance was evaluated using an independent validation dataset and assessed with statistical metrics including coefficient of determination (R^2), root mean square error (RMSE), and mean absolute error (MAE). These metrics indicate the predictive accuracy and generalization ability of each model when applied to unseen data derived from mangrove plots and satellite-based predictors. The results highlight the relative performance differences among algorithms and support the selection of the most reliable model for mapping mangrove carbon stocks in the northern coastal area of Subang.

Estimated Total Carbon Stock and Carbon Sequestration Potential

Spatially explicit mangrove carbon stock was derived by applying the trained machine learning regression model to predict pixel-level total carbon stock (TCS; Mg C ha^{-1}) over the mangrove mask mapped from Sentinel-2 (Equation 6). Pixel predictions were converted to carbon mass using the pixel area (10 m × 10 m = 0.01 ha) and summed across all mangrove pixels to obtain the landscape mangrove carbon stock (MCS). Using this spatial aggregation, the MCS of the study area was estimated at 268,577 Mg C across 2,684 ha of mangrove forest, equivalent to an average of 100 Mg C ha^{-1}, with higher values concentrated in denser stands.

Carbon sequestration is reported here as a CO_2 equivalent potential associated with the standing vegetation carbon stock (AGC + BGC) at the time of assessment rather than an annual sequestration rate. CO_2e was calculated by multiplying MCS (Mg C) by the molecular-weight ratio of CO_2 to C (44/12) (Equation 7), yielding an estimated 984,782 Mg CO_2e for the mapped mangrove extent. Because these totals are produced by spatial upscaling, their uncertainty is influenced by plot-level carbon estimation assumptions (allometry, wood density, and carbon fraction) and mapping/regression errors (mixed pixels, classification accuracy, and prediction residuals).

Discussion

Mangrove and Carbon Potential in Northern Coastal of Subang

Mangroves along the northern coast of Subang are a critical component of coastal vegetation and play a key role in mitigating the adverse effects of oceanographic processes. Field observations indicate that mangroves in the study area exhibit several distribution patterns that reflect their differential responses to the oceanographic dynamics along the shoreline. For instance, Pattern-1 (Figure 5) shows mangrove distribution aligned with the river estuary, driven by sediment accumulation caused by upstream erosion. This process creates new areas suitable for mangrove colonization, particularly for *Avicennia* species, which are highly adaptive to sedimentation. Similarly, Marfi et al. [37] reported the emergence of a new mangrove area of 2,485 ha in the Aceh Tamiang River estuary between 2000 and 2023. Continuous sediment deposition in mangrove ecosystems contributes to vertical soil accretion and increased organic matter accumulation, which are critical for ecosystem capacity and resilience. For example, the vertical accretion rates in the Palau mangrove forest in Vietnam range from 0.47 ± 0.08 cm/year [38]. In the eastern coastal region of Papua, Indonesia, the maximum sediment accumulation reaches 4.4 cm/year or 3.9 g/cm^2/year [39]. While in China, rates range from 10 to 62 kg/m^2/year [40]. Such sedimentation processes provide long-term benefits for the conservation and stabilization of the vulnerable coastline of Java Island under rising sea levels.

The study area hosts 18 mangrove species, five of which are dominant and coincide with the sampling plots. The remaining species are rare, occurring only in limited locations, except for the genus *Acanthus*, which is found along the pond embankments. Notably, the genera *Bruguiera* and *Sonneratia* were also observed, but were extremely rare and considered uncommon in the region. Among the dominant species, *Avicennia marina* and *Rhizophora stylosa* collectively accounted for over 75% of the individuals (Table 3), forming the canopy layer of the mangrove forest. In contrast, species such as *Avicennia alba* are sparse (0.3% at Site-1, Figure 1), whereas *Bruguiera cylindrica* and *Ceriops decandra* occupy the forest understory. The two dominant species contributed to a mangrove tree density of 8,067 ± 5,332 trees ha^{-1} (ranging from 1,900 to 31,600 trees ha^{-1}), which is higher than that reported in earlier studies in the same area, which reported 3,416 trees ha^{-1} across six species [41]. In comparison, the mangrove density in Rembang Regency reached 14,285 trees ha^{-1}, with a minimum of 7,462 trees ha^{-1} [42]. Additionally, the identification of *R. stylosa*, recognizable by characteristic spots on the dorsal side of its leaves, contrasts with prior research [41], which only reported *R. mucronata*. This discrepancy highlights the need for a taxonomic reassessment of *Rhizophora* species distribution in the Subang coastal region.

These patterns can be interpreted as a coupled geomorphic-ecological control on carbon outcomes: sediment delivery at river mouths promotes accretion and stabilizes suitable substrates, which in turn supports denser stands and faster canopy development, whereas pond-margin and abrasion settings tend to produce more fragmented stands with higher edge exposure. In Subang, the dominance of *Avicennia* (foreshore/accretion flats) and *Rhizophora* (pond margins and inundated former ponds) therefore provides a mechanistic link between shore-estuary-pond gradients, stand structure (DBH and stem density), and the observed variability in vegetation carbon (AGC+BGC). Similar process linkages between degradation/restoration, sediment

dynamics, and mangrove carbon stocks have been reported for the northern coast of Java, where recovery trajectories depend strongly on hydrology and substrate stability [43].

To position Subang within the national blue carbon context, it is important to note that Indonesian mangrove carbon stocks vary widely across maturity and management regimes. For example, recent assessments in Java report substantial variability in restored and estuarine mangroves (e.g., Pasarbanggi-Rembang restoration landscapes; Tuntang estuary systems), and remote-sensing-based biomass mapping in the Java Sea region also indicates strong spatial heterogeneity among mangrove patches (e.g., Karimunjawa Islands) [44–46]. At broader Indonesian scales, emission factor syntheses further show consistent ordering of carbon stocks across undisturbed, regenerated, degraded mangroves, and aquaculture conversions, highlighting the importance of disturbance history when interpreting landscape totals [47–48]. Accordingly, we interpret Subang's comparatively high vegetation carbon values as reflecting locally dense stands and species composition, while acknowledging that the small field-sampled area (~0.58 ha; ~0.02% of mapped extent) and mapping/regression uncertainty can propagate into landscape estimates and should be considered when using the results for policy or carbon accounting applications.

The carbon stock of mangroves in the study area, as determined from field sampling, ranged with an average of 183.73 ± 97.04 Mg C ha^{-1}, reaching a maximum total of 497,415 Mg C ha^{-1}. The average diameter at breast height (DBH) of the sampled trees was 6.08 ± 2.46 cm. Sampling covered a total area of 0.59 ha, representing approximately 0.02% of the total mangrove area and accounting for the observed field density. These results are higher than those reported by Rozainah et al. [49] in Peninsular Malaysia, where the total carbon stock (TCS; AGB + BGB) for *Avicennia marina*-dominated forests was 73.32 Mg C ha^{-1} (AGB = 156 Mg ha^{-1}). They also exceed global-scale predictions of 115 ± 7 Mg C ha^{-1}, with a range of 37–255 Mg C ha^{-1} [50]. When examining species-specific contributions, *Rhizophora stylosa* had a higher average TCS of 242.35 ± 83.86 Mg C ha^{-1} (DBH = 6.04 ± 2.96 cm) compared to *Avicennia* species (*A. marina* and *A. alba*), which reached 173.55 ± 98.15 Mg C ha^{-1} (DBH = 6.16 ± 2.42 cm), although the maximum carbon stock was higher in *Avicennia* (Figure 7). This contrasts with Rozainah et al. [49], where *Rhizophora mucronata* had a TCS of 29.21 Mg C ha^{-1} (AGB = 62.16 Mg ha^{-1}), lower than that of *Avicennia marina*. Above-ground carbon (AGC) alone in the present study averaged 130.11 ± 70.36 Mg C ha^{-1} (range: 33.27–357.20 Mg C ha^{-1}), exceeding values reported by Suardana *et al*. [51] in Benoa Bay, Bali (82.07 ± 37.04 Mg C ha^{-1}) and those in southeastern China (12.0–150.2 Mg ha^{-1}) [52]. Specifically, AGC for the dominant species was 123.06 ± 71.39 Mg C ha^{-1} for *Avicennia* and 171.37 ± 60.14 Mg C ha^{-1} for *Rhizophora* (range: 93.74–288.45 Mg C ha^{-1}) (Figure 7), which was lower than that of *Rhizophora apiculata* in Vietnam, which reached 523.6 Mg C ha^{-1} [53]. The total carbon stock across all sampling plots corresponded to a potential carbon sequestration of 455.08 ± 257.97 Mg CO_2e ha^{-1}, ranging from 121.99–1,309.72 Mg CO_2e ha^{-1}. This is lower than the national scale estimates of 702.29 Mg CO_2e ha^{-1} and Java Island-specific values of 599.38 Mg CO_2e ha^{-1} [54], likely reflecting the dominance of secondary mangrove stands with relatively small DBH (6.08 ± 2.46 cm) in the study area.

Mangrove Spatial Distribution Area

Mangroves in Subang Regency, covering an area of 2,684 ha, were delineated using the Random Forest (RF) machine learning algorithm applied to Sentinel-2 MSI imagery acquired in 2025, achieving an overall accuracy (OA) of 84% and a Kappa statistic (KS) of 0.77. In 2024, the mangrove area was reported as 1,972.98 ha with an OA of 90% [55], while in 2021, Subang Regency supported a larger mangrove extent of 2,884 ha with an OA of 82% [56]. These temporal dynamics indicate rapid anthropogenic pressures and coastal land-use changes, consistent with patterns observed in urban mangrove areas, such as Muara Angke in Jakarta, where mangrove extent fluctuates owing to a combination of development pressures and environmental degradation [57]. Additionally, the mangrove mapping results highlighted the dominant role of water indices in differentiating mangroves from non-mangrove areas. In particular, the Modified Normalized Difference Water Index (MNDWI) and Land Surface Water Index (LSWI) exhibited high sensitivity to the presence of water, including puddles surrounding mangrove stands. This finding aligns with previous research [58], which demonstrated that incorporating the MNDWI alongside vegetation indices significantly improves the accuracy of mangrove mapping.

Because these area estimates were produced by different studies that may use distinct sensors, spatial resolutions, classification algorithms, and validation designs, the inter-annual comparison should be interpreted as indicative rather than strictly like for like. Recent reviews have emphasized that inconsistencies in definitions, proxies, and processing choices can blur the distinction between true mangrove change and methodological artifacts, especially in mixed wet–dry coastal settings [59]. Accordingly, we report the 2025 Sentinel-2/RF map as the primary baseline for this study, and we frame previously published extents as

contextual benchmarks rather than direct change estimates. In silvofishery-dominated landscapes, spectral confusion between mangroves, aquaculture ponds, mudflats, and transient shallow water is a recognized source of commission/omission errors, and water-sensitive indices (e.g., MNDWI, LSWI) may partly capture the tidal inundation state around the canopy edge. Practical guidance for fine-scale mangrove mapping therefore recommends explicit cloud/shadow masking, temporal compositing, and (where possible) controlling for tidal stage or using multi-date imagery to reduce inundation-driven misclassification [60]. These considerations are particularly relevant for Java's dynamic north coast, where coastal inundation and rapid shoreline changes can alter the water vegetation signal at short timescales [61].

In terms of mangrove distribution based on mapping results and field observations, mangroves are predominantly concentrated at river mouths that receive sediment input from upstream rivers. In other landscape types, mangroves are primarily found within aquaculture pond areas employing silvofishery systems that help mitigate the impacts of coastal degradation. These silvofishery systems are distributed extensively across Site-3 and Site-4 (Figure 8). Similar findings were reported by Suwanto *et al*. [41], who observed that mangroves in this region are closely associated with aquaculture activities and restoration efforts in the region. The interrelationship between mangroves, aquaculture ponds, and rehabilitation initiatives has also been documented in Muara Angke, where mangrove ecosystem sustainability is heavily influenced by the integration of ecological functions, coastal economic activities, and regional management policies [57]. The loss of mangrove cover in these areas has contributed to increased vulnerability to sea-level rise, which poses a risk of submerging aquaculture ponds in the future. Specifically, Site-2 and Site-3 (Figure 1) experienced the most severe coastal abrasion in Subang, attributable to the decline of mangroves as natural barriers against shoreline erosion and rising seas. Between 2010 and 2020, these sites were identified as the areas most affected by abrasion [62]. Similarly, Rahmawati *et al.* [63] reported that in Bekasi Regency, located west of the study area, mangrove loss led to land erosion and the submergence of northern ponds due to sea-level rise. Additional threats include the development of port infrastructure and industrial zones in the easternmost portion of the study area, which has impacted mangrove coverage at Site-1 (Figure 1).

Mangrove Carbon Stock Modelling and Machine Learning Performance

This study demonstrates the promise of data-driven models for mangrove carbon estimation, but the discussion is reframed to emphasize regression diagnostics (R^2, RMSE, and MAE) rather than accuracy percentages. We explicitly distinguished training performance from independent validation performance and interpreted the observed decline in R^2 from training to validation as evidence of limited generalization, which is commonly amplified in geospatial machine learning when training and test samples are spatially dependent [64,54]. Accordingly, the revised text clarifies that model selection was based on validation errors and stability across folds, and it positions our validation results within the range reported by recent Sentinel-2 mangrove biomass/carbon studies using machine learning (e.g., [66–68]). The ecological interpretation of the predictors was also strengthened. Vegetation indices such as MNDVI and DVI are proxies for canopy vigor, leaf area, and (indirectly) stand structure, which can relate non-linearly to biomass and carbon through saturation and mixed pixel effects in dense mangroves. In contrast, the prominence of water-related indices in some models (e.g., MNDWI/LSWI) is interpreted cautiously because these predictors can capture tidal inundation and background water signals that co-vary with mangrove zonation and edge density rather than biomass alone, especially in intertidal settings [69]. Therefore, differences in predictor stability across RF, SVM, and CART are interpreted as robust signals, where models that rely heavily on hydrology/edge proxies may be less transferable across seasons or tide states. Thus, uncertainty and operational transferability are explicitly acknowledged in the revised discussion [64,65].

Carbon Potential of Mangrove

Based on the upscaled predictions, the total mangrove vegetation carbon in Subang was estimated at 268,577 Mg C (≈100 Mg C ha^{-1} across 2,684 ha), derived by predicting pixel-level TCS (Mg C ha^{-1}) from the trained regression model(s) and aggregating across all pixels classified as mangrove. This stock was converted to a CO_2-equivalent potential of 984,782 Mg CO_2e using the molecular weight ratio (44/12), which represents the atmospheric CO_2 associated with the standing vegetation carbon pool at the time of assessment (AGC+BGC), not an annual sequestration rate. We interpret this landscape as totally conservative because generalization performance declined in independent validation relative to training, which can occur when spatial autocorrelation and limited sample sizes inflate apparent performance if training and test data are not spatially independent [64,65]. Comparisons with other studies were refined by explicitly distinguishing between carbon pools and methods. Our estimates focused on vegetation carbon (AGC+BGC) and did not include soil organic carbon (SOC), which can dominate the total ecosystem carbon in mangroves. For

example, recent Indonesian field assessments in aquaculture-impacted settings reported SOC far exceeding vegetation pools [70]. National syntheses likewise show strong variation in total ecosystem carbon across Indonesian mangrove management regimes and highlight the importance of transparent pool definitions for MRV and policy use [47]. Accordingly, the differences between Subang and other Indonesian or global values should be interpreted considering the sensor resolution, predictor sets, validation design, and whether SOC is included.

Limitation and Recommendation

This study has several limitations, primarily related to the scope of the data, which was restricted to measurements of mangrove vegetation carbon stocks. In reality, assessing the role of mangrove ecosystems in climate change through blue carbon indicators requires consideration of multiple carbon pools, including soil organic carbon (SOC) contained in sediments and mud [71]. The high production of mangrove litter continuously contributes to carbon accumulation in sediments; however, tidal dynamics cause a portion of this carbon to be exported to surrounding aquatic zones [72,73]. Such dynamic changes necessitate measurements that capture the vertical structure of vegetation and its contribution to carbon sequestration. SOC is particularly critical, serving as a key indicator in carbon cycle studies aimed at mitigating greenhouse gas emissions by tracing carbon from the canopy to organic matter in sediments [74]. Studies by Rozainah *et al.* [49] and Malik *et al.* [70] indicate that more than 80% of carbon in mangrove blue carbon ecosystems is stored in the soil. At a global scale, SOC is estimated at 5.00 ± 0.94 Pg C, or 703 ± 38 Mg C ha^{-1}, assuming a sediment depth of 1 meter [75]. Therefore, future research incorporating soil carbon measurements is urgently needed to provide comprehensive and reliable data to inform sustainable coastal management policies.

The application of machine learning in this study demonstrated the robustness of these algorithms in predicting mangrove carbon stocks. However, the relatively low R-squared values obtained in the validation tests highlight the need for further optimization of the employed machine learning models. Moreover, the substantial discrepancy between the training and validation results suggests the occurrence of overfitting (Figures 10 and 12), underscoring the necessity for additional model refinement. For instance, previous studies have successfully applied Particle Swarm Optimization (PSO) to enhance the performance of machine learning algorithms, improving R-squared values during validation and mitigating overfitting [76,77]. Furthermore, incorporating alternative machine learning algorithms that have demonstrated effectiveness in prior research could increase the likelihood of achieving more accurate results. Another promising approach involves leveraging high-resolution drone (UAV) imagery to estimate mangrove carbon stocks, offering complementary insights alongside satellite-based analyses [77,78].

Mangrove conservation efforts in the study area are essential for protecting coastal landscapes from oceanographic hazards. These efforts represent a cost-effective contribution to national and global emission reduction strategies [75,79,80]. At the species level, three ecologically important and relatively rare genera, *Ceriops*, *Bruguiera*, and *Sonneratia*, were identified within the study area. These genera exhibit limited local distributions and are rarely found in other locations within the region. Consequently, targeted conservation interventions, including protection and replanting within designated protected habitats, are necessary to prevent local extinction, particularly in response to potential future pond conversion in natural habitats. Mangrove restoration activities should be implemented in ecologically suitable areas by carefully considering the local biophysical conditions and oceanographic parameters. Specifically, areas characterized by high sedimentation rates, as observed in Pattern-1 (Figure 5), particularly at Site-1 (Figure 1), are suitable for mangrove establishment and can be utilized to accelerate the expansion of *Avicennia* species. Former aquaculture ponds that have become permanently inundated owing to sea-level rise and coastal abrasion (Pattern-3 in Figure 5; Sites-2 and 3 in Figure 1) are suitable for restoration using species from the *Rhizophora* genus. Such efforts require appropriate planting techniques, including the physical formation of *Rhizophora* root structures during the nursery stage of development. Furthermore, in areas exposed to relatively strong wave energy, such as Sites-3 and 4 (Figure 1), corresponding to Pattern-4 (Figure 5), *Rhizophora* species have been demonstrated to be particularly effective in enhancing coastal protection.

From an economic perspective, silvofishery-based coastal landscape conservation represents a viable approach to reconciling economic livelihoods and climate policy objectives. In the study area, two silvofishery systems have been historically implemented: (i) silvofishery with active mangrove planting, predominantly using *Rhizophora* species, and (ii) silvofishery that preserves existing mangrove vegetation during pond construction, primarily involving *Avicennia* species. In terms of effectiveness, further research is required to distinguish the relative impacts of these systems on both carbon sequestration and the economic outcomes.

These findings underscore the importance of selecting conservation and management strategies that align with the biophysical characteristics of the coastal landscape. Such alignment is critical for achieving sustainable coastal management and supporting climate adaptation and mitigation efforts in Indonesia. This is particularly relevant to the role of mangroves in the study area in the context of national policy, including the FOLU Net Sink 2030 program (Forestry and Other Land Use), as well as Indonesia's commitments under its Nationally Determined Contribution (NDC) framework [81,82].

Conclusions

This study quantified mangrove distribution, carbon stock, and carbon sequestration potential in the northern coastal region of Subang Regency using Sentinel-2 imagery and machine learning methods. Mangroves cover approximately 2,684 ha, with an overall accuracy of 84% and a Kappa statistic of 0.77 based on a Random Forest model. Field-based measurements indicated an average vegetation carbon stock of 183.73 ± 97.04 Mg C ha^{-1}, reflecting substantial spatial variability across sites with differing stand densities and geomorphic conditions. Among the evaluated models, linear SVM demonstrated the most stable predictive performance during validation (R^2 = 0.88), whereas CART and RF exhibited indications of overfitting. The estimated total vegetation carbon stock reached 268,577 Mg C, corresponding to a cumulative potential emission equivalent of 984,782 Mg CO_2e, although these values exclude soil organic carbon and therefore represent conservative estimates. Overall, the findings demonstrate that integrating medium-resolution satellite data with machine learning techniques can provide a robust and spatially explicit assessment of mangrove carbon stocks to support evidence-based coastal ecosystem management in the future.

Author Contributions

NS: Conceptualization, Funding acquisition, Methodology, Supervision, Data interpretation, Writing - Review & Editing; **RA'A:** Investigation, Field survey, Data curation, Formal analysis; **AU:** Investigation, Field survey, Data curation, Formal analysis; **AR:** Data supervision, Formal analysis, Writing - Original Draft, Manuscript formatting; **O:** Data supervision, Formal analysis, Visualization, Writing - Review & Editing; and **YR:** Writing - Review & Editing, Manuscript formatting.

AI Writing Statement

During the preparation of this work, the authors used *Gemini AI* to assist in generating the initial visual layout of Figure 3. After using this tool, the authors reviewed, refined, and edited the generated output by adding manual drawings and adjustments to ensure scientific accuracy and clarity. The authors take full responsibility for the final content of the publication.

Conflicts of interest

There are no conflicts to declare.

Acknowledgments

The authors would like to express their gratitude to all parties who supported this research. Special appreciation is extended to the field survey team for their assistance in mangrove data collection along the northern coast of Subang Regency. The authors also thank the institutions and data providers that facilitated access to satellite imagery and environmental datasets used in this study.

References

1. Barbier, E.B.; Hacker, S.D.; Kennedy, C.; Koch, E.W.; Stier, A.C.; Silliman, B.R. The Value of Estuarine and Coastal Ecosystem Services. *Ecol. Monogr*. **2011**, *81*(2), 169–193, doi: 10.1890/10-1510.1.
2. Friess, D.A.; Rogers, K.; Lovelock, C.E.; Krauss, K.W.; Hamilton, S.E.; Lee, S.Y.; Lucas, R.; Primavera, J.; Rajkaran, A.; Shi, S. The State of the World's Mangrove Forests: Past, Present, and Future. *Annu. Rev. Environ. Resour*. **2019**, *44*(1), 89–115, doi: 10.1146/annurev-environ-101718-033302.
3. Spalding, M.; Kainuma, M.; Collins, L. *World Atlas of Mangroves*; Earthscan: London, UK, 2010, ISBN 978-1-84407-657-4.
4. Alongi, D.M. Carbon Cycling and Storage in Mangrove Forests. *Ann. Rev. Mar. Sci.* **2014**, *6*(1), 195–219, doi: 10.1146/annurev-marine-010213-135020.
5. Donato, D.C.; Kauffman, J.B.; Murdiyarso, D.; Kurnianto, S.; Stidham, M.; Kanninen, M. Mangroves Among The Most Carbon-Rich Forests in The Tropics. *Nat. Geosci*. **2011**, *4*(5), 293–297, doi: 10.1038/ngeo1123.
6. McLeod, E.; Chmura, G.L.; Bouillon, S.; Salm, R. A Blueprint for Blue Carbon: Toward an Improved Understanding of the Role of Vegetated Coastal Habitats in Sequestering CO_2. *Front. Ecol. Environ*. **2011**, *9*(10), 552–560, doi: 10.1890/110004.
7. Giri, C.; Ochieng, E.; Tieszen, L.L.; Zhu, Z. Status and Distribution of Mangrove Forests of the World Using Earth Observation Satellite Data. *Global Ecology and Biogeography*. **2011**, *20*(1), 154–159, doi: 10.1111/j.1466-8238.2010.00584.x.
8. Drusch, M.; Bello, U.D.; Carlier, S.; Colin, O.; Fernandez, V.; Gascon, F.; Hoersch, B.; Isola, C.; Laberinti, P.; Martimort, P.; et al. Sentinel-2: ESA's Optical High-Resolution Mission for GMES Operational Services, *Remote Sens. Environ*. **2012**, *120*, 25–36, doi: 10.1016/j.rse.2011.11.026.
9. Hamilton, S.E.; Casey, D. Creation of a High Spatio-Temporal Resolution Global Database of Continuous Mangrove Forest Cover for the 21st Century (CGMFC-21). *Global Ecology and Biogeography* **2016**, *25*(6), 729–738, doi: 10.1111/geb.12449.
10. Simarmata, N.; Wikantika, K.; Darmawan, S.; Harto, A.B.; Sakti, A.D.; Santo, A.A. Mangrove Ecosystem Species Mapping from Integrated Sentinel-2 Imagery and Field Spectral Data Using Random Forest Algorithm. *J. Appl. Remote Sens*. **2024**, *18*(1), doi: 10.1117/1.JRS.18.014509.
11. Zhang, H.; Xia, Q.; Dai, S.; Zheng, Q.; Zhang, Y.; Deng, X. Mangrove Forest Mapping from Object-Oriented Multi-Feature Ensemble Classification Using Sentinel-2 Images. *Front. Mar. Sci*. **2023**, *10*, doi: 10.3389/fmars.2023.1243116.
12. Ipranta, I.; Mawardi, S.; Hanafi, M.; Christiana, I. Karakteristik Kawasan Pesisir Pantai Cilamaya (Teluk Blanakan dan Teluk Ciasem), Kabupaten Subang, Propinsi Jawa Barat. *Jurnal Geologi Kelautan* **2021**, *19*(1), doi: 10.32693/jgk.19.1.2021.667.
13. Narendra B.H.; Siringoringo, H.H.; Siregar, C.A. Gis Based Flood Hazard and Vulnerability Mapping: a Case Study of Tidal and River Floods in Downstream of Ciasem Watershed, Subang, West Java. *Indonesian Journal of Forestry Research* **2017**, *4*(1), 37–48, doi: 10.20886/ijfr.2017.4.1.37-48.
14. (BMKG) *Badan Meteorologi, Klimatologi, dan Geofisika*/Meteorological, Climatological, and Geophysical Agency. Prakiraan Pasang Surut (Maritim BMKG). Available online: https://maritim.bmkg.go.id/cuaca/pasut.
15. Rouse, W.; Haas, H.; Schell, J.A.; Deering, W. Monitoring Vegetation Systems in the Great Plains with ERTS. *NASA Goddard Space Flight Center* **1974**, *1*, 309–317.
16. Kaufman, Y.J.; Tanre, D.; Atmospherically Resistant Vegetation Index (ARVI) for EOS-MODIS. *IEEE Transactions on Geoscience and Remote Sensing* **1992**, *30*(2), 261–270, doi: 10.1109/36.134076.
17. Huete, A.R. A Soil-Adjusted Vegetation Index (SAVI). *Remote Sens. Environ*. **1998**, *25*(3), 295–309, doi: 10.1016/0034-4257(88)90106-X.
18. Tucker, C.J. Red and Photographic Infrared Linear Combinations for Monitoring Vegetation. *Remote Sens. Environ*. **1979**, *8*(2), 127–150, doi: 10.1016/0034-4257(79)90013-0.
19. Huete, A.; Didan, K.; Miura, T.; Rodriguez, E.P.; Gao, X.; Ferreira, L.G. Overview of the Radiometric and Biophysical Performance of the MODIS Vegetation Indices. *Remote Sens. Environ*. **2002**, *83*(1–2), 195–213, doi: 10.1016/S0034-4257(02)00096-2.

20. Gitelson, A.A.; Kaufman, Y.J.; Merzlyak, M.N. Use of a Green Channel in Remote Sensing of Global Vegetation from EOS-MODIS. *Remote Sens. Environ*. **1996**, *58*(3), 289–298, doi: 10.1016/S0034-4257(96)00072-7.
21. Jurgens, C. The Modified Normalized Difference Vegetation Index (MNDVI) - a New Index to Determine Frost Damages in Agriculture Based on Landsat TM Data. *Int. J. Remote Sens*. **1997**, *18*(17), 3583–3594, doi: 10.1080/014311697216810.
22. Lymburner, L.; Beggs, P.; Jacobson, C. Estimation of Canopy-Average Surface-Specific Leaf Area Using Landsat TM Data. *Photogramm. Eng. Remote Sensing*. **2000**, *66*, 183–191.
23. Mishra, S.; Mishra, D.R. Normalized Difference Chlorophyll Index: a Novel Model for Remote Estimation of Chlorophyll-A Concentration in Turbid Productive Waters. *Remote Sens. Environ*. **2012**, *117*, 394–406, doi: 10.1016/j.rse.2011.10.016.
24. McFetters, S.K. The Use of the Normalized Difference Water Index (NDWI) in the Delineation of Open Water Features. *Int. J. Remote Sens*. **1996**, *17*(7), 1425–1432, doi: 10.1080/01431169608948714.
25. Xu, H. Modification of Normalised Difference Water Index (NDWI) to Enhance Open Water Features in Remotely Sensed Imagery. *Int. J. Remote Sens*. **2006**, *27*(14), 3025–3033, doi: 10.1080/01431160600589179.
26. Rad, A.M.; Kreitler, J.; Sadegh, M. Augmented Normalized Difference Water Index for Improved Surface Water Monitoring. *Environmental Modelling & Software* **2021**, *140*, 105030, doi: 10.1016/j.envsoft.2021.105030.
27. Xiao, X. *et al.* Satellite-Based Modeling of Gross Primary Production in an Evergreen Needleleaf Forest. *Remote Sens. Environ.* **2004**, *89*(4), 519–534, doi: 10.1016/j.rse.2003.11.008.
28. Zha Y.; Gao J.; Ni S. Use of Normalized Difference Built-Up Index in Automatically Mapping Urban Areas from TM Imagery. *Int. J. Remote Sens*. **2003**, *24*(3), 583–594, doi: 10.1080/01431160304987.
29. Shih Y-J.; Liu, K.; Huang, S-C.; Chang, Yi.; Ji, F-F.; Cao, C-X.; Ye, M-X.; Li, Y-M.; Jin, Y-H.; Yao, Y-R. Multiple Methods Reveal the Carbon Stock Potential of Young Reforested Mangroves in Quanzhou Bay Nature Reserve. China, *Ecol. Indic*. **2025**, *178*, 114126, doi: 10.1016/j.ecolind.2025.114126.
30. Komiyama, A.; Poungparn, S.; Kato, S. Common Allometric Equations for Estimating the Tree Weight of Mangroves. *J. Trop. Ecol*. **2005**, *21*(4), 471–477, doi: 10.1017/S0266467405002476.
31. Dharmawan, I.W.S.; Siregar, C.A. Karbon Tanah dan Pendugaan Karbon Tegakan *Avicennia Marina* (Forsk.) Vierh. di Ciasem, Purwakarta. *Jurnal Penelitian Hutan dan Konservasi Alam* **2008**, *5*(4), pp. 317–328, doi: 10.20886/jphka.2008.5.4.317-328.
32. Analuddin, K.; Kadidae, L.A.; Haya, L.O.M.Y.; Septiana, A.; Sahidin, I.; Syahrir, A.; Rahim, S.; Fajar, L.O.A.; Nadaoka, K. Aboveground Biomass, Productivity and Carbon Sequestration in *Rhizophora Stylosa* Mangrove Forest of Southeast Sulawesi, Indonesia. *Biodiversitas* **2020**, *21*(4), doi: 10.13057/biodiv/d210407.
33. Maung, W.S.; Tsuyuki, S.; Hiroshima, T.; Htay, S.S. Assessing Above Ground Biomass of Wunbaik Mangrove Forest in Myanmar Using Machine Learning and Remote Sensing Data. *Discover Conservation* **2025**, *2*(1), 8, doi: 10.1007/s44353-025-00025-3.
34. Muñoz A.S.M; Alvis, Á.I.G.; Martínez I.F.B. A Random Forest Model to Predict Soil Organic Carbon Storage in Mangroves from Southern Colombian Pacific Coast. *Estuar. Coast. Shelf Sci*. **2024**, *299*, 108674, doi: 10.1016/j.ecss.2024.108674.
35. Johnson, K.; Kuhn, M. What They Forgot to Tell You About Machine Learning with an Application to Pharmaceutical Manufacturing. *Pharmaceutical Statistics* **2025**, *24*(1), e2366, doi: 10.1002/pst.2366
36. Przemyslaw, B. DALEX: Explainers for Complex Predictive Models in R. *Journal of Machine Learning Research* **2018,** *19*(84), 1–5.
37. Marfi, K.P.; Asy'Ari, R.; Rahmawati, A.D.; Dzulfigar, A.; Ulfa, A.; Puspitasari, F.R.; Setiawan, Y.; Zamani, N.P.; Pramulya, R. Dynamic Change of Mangroves in Aceh Tamiang Regency using Landsat Temporal Data, 2000 to 2023. *Media Konservasi* **2025**, *30*(2), 344, doi: 10.29244/medkon.30.2.344.
38. MacKenzie, R.A.; Foulk, P.B.; Klump, J.V.; Weckerly, K.; Purbospito, J.; Muldiyarso, D.; Donato, D.C.; Nam, V.N. Sedimentation and Belowground Carbon Accumulation Rates in Mangrove Forests that Differ in

Diversity and Land Use: a Tale of Two Mangroves. *Wetl. Ecol. Manag*. **2016**, *24*(2), 245–261, doi: 10.1007/s11273-016-9481-3.

39. Walsh, J.P.; Nittrouer, C.A. Mangrove-bank Sedimentation in a Mesotidal Environment with Large Sediment Supply, Gulf Of Papua. *Mar. Geol*. **2004**, *208*(2–4), 225–248, doi: 10.1016/j.margeo.2004.04.010.
40. Alongi, D.M.; Pfitzner, J.; Trott, L.A.; Tirendi, F.; Dixon, P.; Klumpp, D.W. Rapid Sediment Accumulation and Microbial Mineralization in Forests of the Mangrove Kandelia Candel in the Jiulongjiang Estuary, China. *Estuar. Coast. Shelf Sci*. **2005**, *63*(4), 605–618, doi: 10.1016/j.ecss.2005.01.004.
41. Suwanto, A.; Takarina, N.D.; Koestoer, R.H.; Frimawaty, E. Diversity, Biomass, Covers, and NDVI Of Restored Mangrove Forests in Karawang and Subang Coasts, West Java, Indonesia. Biodiversitas **2021**, *22*(9), doi: 10.13057/biodiv/d220960.
42. Hendrarto, I.B.; Nitisuparjo, M. Biodiversity of Benthic Diatom and Primary Productivity of Benthic Micro-Flora In Mangrove. *Journal of Coastal Development* **2011**, *14*(1), 131–140.
43. Ardhani, T.S.P.; Sasmito, S.D.; Murdiyarso, D.; Jennerjahn, T.C.; Krauss, K.W. Restoration of declining soil carbon stocks and lost surface elevations in degraded mangroves on the northern coast of Java, Indonesia. *Frontiers in Ecology and Evolution* **2025**, *13*, doi:10.3389/fevo.2025.1448702.
44. Wirasatriya, A.; Pribadi, C.B.; Helmi, M.; Wicaksono, P.; Sasmito, S.D. Mangrove Above-Ground Biomass and Carbon Stock in the Karimunjawa–Kemujan Islands Estimated from Unmanned Aerial Vehicle Imagery. *Sustainability* **2022**, *14*, 706, doi: 10.3390/su14020706.
45. Soeprobowati, T.R.; Supriharyono; Purnomo, P.W.; Sugianto, D.N.; Suryono, S. The Carbon Stock Potential of the Restored Mangrove Ecosystem of Pasarbanggi, Rembang, Central Java. *Marine Environmental Research* **2024**, *193*, 106257, doi: 10.1016/j.marenvres.2023.106257.
46. Rahim, A.; Soeprobowati, T.R.; Putranto, T.T.; Al Falah, M.H.; Gell, P. Contribution of Mangrove Forest Carbon Stocks on Climate Change Mitigation: A Case Study at Tuntang Estuary, Central Java. *Journal of Coastal Conservation* **2024**, *28*, 65, doi: 10.1007/s11852-024-01059-w.
47. Murdiyarso, D.; Krisnawati, H.; Adinugroho, W.C.; Sasmito, S.D. Deriving Emission Factors for Mangrove Blue Carbon Ecosystem in Indonesia. *Carbon Balance and Management* **2023**, *18*, 12, doi: 1186/s13021-023-00233-1
48. Royna, M.; Sidik, F.; Wardiatno, Y.; Lovelock, C.E.; Alongi, D.M. Carbon Stocks and Effluxes in Mangroves Converted into Aquaculture: A Case Study from Banten Province, Indonesia. *Frontiers in Ecology and Evolution* **2024**, *12*, doi: 10.3389/fevo.2024.1340531
49. Rozainah, M.Z.; Nazri, M.N.; Sofawi, A.B.; Hemati, Z.; Juliana, W.A. Estimation of Carbon Pool in Soil, Above and Below Ground Vegetation at Different Types of Mangrove Forests in Peninsular Malaysia. *Marine Pollution Bulletin* **2018**, *137*, 237–245. doi:10.1016/j.marpolbul.2018.10.023.
50. Kauffman, J.B.; Bernardino, A.F.; Ferreira, T.O.; Bolton, N.W.; Gomes, L.E.O.; Nobrega, G.N. Total Ecosystem Carbon Stocks of Mangroves across Broad Global Environmental and Physical Gradients. *Ecological Monographs* **2020**, *90*, doi:10.1002/ecm.1405.
51. Suardana, I.W.; Siregar, V.P.; Wouthuyzen, S.; Nababan, B.; Adrianto, L. Estimation and Mapping Above-Ground Mangrove Carbon Stock Using Sentinel-2 Data Derived Vegetation Indices in Benoa Bay of Bali Province, Indonesia. *Forest and Society* **2023**, *7*, 116–134, doi:10.24259/fs.v7i1.22062.
52. Meng, Y.; Li, Y.; Gao, J.; Chen, J.; Zhu, X. Relationships between Above- and Below-Ground Carbon Stocks in Mangrove Forests Facilitate Better Estimation of Total Mangrove Blue Carbon. *Carbon Balance and Management* **2021**, *16*, 8, doi:10.1186/s13021-021-00172-9.
53. Van Vinh, T.; Marchand, C.; Linh, T.V.K.; Vinh, D.D.; Allenbach, M. Allometric Models to Estimate Above-Ground Biomass and Carbon Stocks in *Rhizophora apiculata* Tropical Managed Mangrove Forests (Southern Vietnam). *Forest Ecology and Management* **2019**, *434*, 131–141, doi:10.1016/j.foreco.2018.12.017.
54. Maulana, M.I.; Auliah, N.L.; Onrizal. Potential Carbon Storage of Indonesian Mangroves. *IOP Conference Series: Earth and Environmental Science* **2021**, *782*, 032014, doi:10.1088/1755-1315/782/3/032014.

55. Dzulfigar, A.; Asy'ari, R.; Rahmawati, A.D.; Madinu, A.M.A.; Nugraha, A.L. Spatio-Temporal Analysis of Mangroves in Subang Regency Using Sentinel-2 Time-Series Data. *SSRS Journal A: Agro-Environmental Research* **2024**, *2*, 28–47.
56. Asy'Ari, R.; Dzulfigar, A.; Rahmawati, A.D.; Madinu, A.M.A.; Nugraha, A.L. Mapping Mangrove Forest Distribution on Banten, Jakarta, and West Java Ecotone Zone from Sentinel-2-Derived Indices Using Cloud Computing Based Random Forest. *Journal of Natural Resources and Environmental Management* **2022**, *12*, 97–111, doi:10.29244/jpsl.12.1.97-111.
57. Santoso, N.; Oktovianus; Rachmatullah, A.; Oktavia, R.C.D.; Suprajanti, D.S.; Avenzora, R. An Integrative Assessment of a Mangrove Ecosystem: Sustainability and Management in Muara Angke, Jakarta. *Sustainability* **2026**, *18*, 464, doi:10.3390/su18010464.
58. Asy'ari, R.; Dzulfigar, A.; Rahmawati, A.D.; Madinu, A.M.A.; Nugraha, A.L. Mangrove Damage vs Succession: An Opinion on the Journey of Mangrove Investigation Studies in Subang Regency Coast Area. *SSRS Journal A: Agro-Environmental Research* **2023**, *1*, 1–6.
59. Wei, S.; Zhang, H.; Ling, J. A Review of Mangrove Degradation Assessment Using Remote Sensing: Advances, Challenges, and Opportunities. *GIScience & Remote Sensing* **2025**, *62*, doi:10.1080/15481603.2025.2491920.
60. Schill, S.R.; McNulty, V.P.; Perez, D.; Shono, K.; Friedman, K. *Remote Sensing Techniques for Mapping and Monitoring Mangroves at Fine Scales*; FAO: Rome, Italy, **2024**, doi:10.4060/cd0823en.
61. Wiguna, E.A.; Wirasatriya, A.; Helmi, M.; Pribadi, C.B.; Sugianto, D.N. Shoreline extraction on Java's North Coast based on the satellite imagery: utilizing U-Net segmentation across diverse coastal characteristics. *Earth Science Informatics* **2025**, *18*, 534, doi:10.1007/s12145-025-02022-5.
62. Madinu, A.M.A.; Asy'ari, R.; Dzulfigar, A.; Rahmawati, A.D.; Nugraha, A.L. Monitoring of coastal dynamics at Subang Regency using Landsat Collection Data and Cloud Computing Based. *BIO Web of Conferences* **2024**, *106*, 04005, doi:10.1051/bioconf/202410604005.
63. Rahmawati, A.D.; Asy'ari, R.; Dzulfigar, A.; Madinu, A.M.A.; Nugraha, A.L. Spatiotemporal Analysis of Mangrove in Subang Regency using Sentinel-2 Timeseries Data. *SSRS Journal A: Agro-Environmental Research* **2024**, *2*, 48–59.
64. Karasiak, N.; Dejoux, J.-F.; Monteil, C.; Sheeren, D. Spatial dependence between training and test sets: another pitfall of classification accuracy assessment in remote sensing. *Machine Learning* **2022**, *111*, 2715–2740, doi:10.1007/s10994-021-05972-1.
65. Kattenborn, T.; Schiefer, F.; Frey, J.; Feilhauer, H.; Mahecha, M.D.; Dormann, C.F. Spatially autocorrelated training and validation samples inflate performance assessment of convolutional neural networks. *ISPRS Open Journal of Photogrammetry and Remote Sensing* **2022**, *5*, 100018, doi:10.1016/j.ophoto.2022.100018.
66. Pham, T.D.; Yoshino, K.; Nguyen, T.T.; Bui, D.T.; Nguyen, H.T. Estimating Mangrove Above-Ground Biomass Using Extreme Gradient Boosting Decision Trees Algorithm with Fused Sentinel-2 and ALOS-2 PALSAR-2 Data in Can Gio Biosphere Reserve, Vietnam. *Remote Sensing* **2020**, *12*, 777, doi:10.3390/rs12050777.
67. Farzanmanesh, R.; Khoshelham, K.; Volkova, L.; Thomas, S.; Ravelonjatovo, J.; Weston, C.J. Quantifying Mangrove aboveground biomass changes: Analysis of conservation impact in blue forests projects using Sentinel-2 satellite imagery. *Forest Ecology and Management* **2024**, *561*, 121920, doi:10.1016/j.foreco.2024.121920.
68. Peng, C.; Li, Y.; Zhang, X.; Liu, J.; Wang, Y. Estimating coastal mangrove aboveground biomass of Zhejiang province based on Sentinel-2 images and multiple machine learning algorithms. *Frontiers in Forests and Global Change* **2025**, *8*, doi:10.3389/ffgc.2025.1662546.
69. Hickey, S.M.; Radford, B. Turning the Tide on Mapping Marginal Mangroves with Multi-Dimensional Space–Time Remote Sensing. *Remote Sensing* **2022**, *14*, 3365, doi:10.3390/rs14143365.
70. Malik, A.; Fensholt, R.; Mertz, O.; Rahman, A.A.; Sidik, F. Mangrove blue carbon stocks estimation in South Sulawesi Indonesia. *Continental Shelf Research* **2023**, *269*, 105139, doi:10.1016/j.csr.2023.105139.

71. Asilo, H.A.M.; Yap-Dejeto, L.G. Understanding blue carbon management strategies: quantitative assessment of blue carbon stock among three mangrove stands in Eastern Visayas, Philippines. *Carbon Research* **2025**, *4*, 63, doi:10.1007/s44246-025-00216-6.
72. Kristensen, E.; Bouillon, S.; Dittmar, T.; Marchand, C. Organic carbon dynamics in mangrove ecosystems: A review. *Aquatic Botany* **2008**, *89*, 201–219, doi:10.1016/j.aquabot.2007.12.005.
73. Yong, Y.; Baipeng, P.; Guangcheng, C.; Yan, C. Processes of organic carbon in mangrove ecosystems. *Acta Ecologica Sinica* **2011**, *31*, 169–173, doi:10.1016/j.chnaes.2011.03.008.
74. Pham, T.D.; Yoshino, K.; Nguyen, T.T.; Bui, D.T.; Nguyen, H.T. Improvement of Mangrove Soil Carbon Stocks Estimation in North Vietnam Using Sentinel-2 Data and Machine Learning Approach. *GIScience & Remote Sensing* **2021**, *58*, 68–87, doi:10.1080/15481603.2020.1857623.
75. Jardine, S.L.; Siikamäki, J.V. A global predictive model of carbon in mangrove soils. *Environmental Research Letters* **2014**, *9*, 104013, doi:10.1088/1748-9326/9/10/104013.
76. Huang, Z.; Zhang, Y.; Chen, X.; Li, J.; Wang, H. Estimating mangrove above-ground biomass at Maowei Sea, Beibu Gulf of China using machine learning algorithm with Sentinel-1 and Sentinel-2 data. *Geocarto International* **2022**, *37*, 15778–15805, doi:10.1080/10106049.2022.2102226.
77. Gülci, S.; Akay, A.E.; Aricak, B.; Sariyildiz, T. Recent Advances in UAV-Based Structure-from-Motion Photogrammetry for Aboveground Biomass and Carbon Storage Estimations in Forestry. In *Concepts and Applications of Remote Sensing in Forestry*; Springer Nature: Singapore, **2022**; pp. 395–409, doi:10.1007/978-981-19-4200-6_20.
78. Wang, Z.; Li, X.; Zhang, Y.; Chen, J.; Liu, H. Regional mangrove vegetation carbon stocks predicted integrating UAV-LiDAR and satellite data. *Journal of Environmental Management* **2024**, *368*, 122101, doi:10.1016/j.jenvman.2024.122101.
79. Jakovac, C.C.; Latawiec, A.E.; Papp, L.; Crouzeilles, R.; Ferreira, M.S.; Strassburg, B.B.N. Costs and Carbon Benefits of Mangrove Conservation and Restoration: A Global Analysis. *Ecological Economics* **2020**, *176*, 106758, doi:10.1016/j.ecolecon.2020.106758.
80. Zeng, Y.; Friess, D.A.; Sarira, T.V.; Siman, K.; Koh, L.P. Global Potential and Limits of Mangrove Blue Carbon for Climate Change Mitigation. *Current Biology* **2021**, *31*(8), 1737-1743.e3, doi: 10.1016/j.cub.2021.01.070.
81. Arifanti, V.B.; Candra, R.A.; Putra, C.A.S.; Asyhari, A.; Gangga, A.; Ritonga, R.A; Ilman, M.; Anggoro, A.W.; Novita, N. Greenhouse Gas Fluxes of Different Land Uses in Mangrove Ecosystem of East Kalimantan, Indonesia. *Carbon Balance Manag*. **2024**, *19*(1), 17, doi: 10.1186/s13021-024-00263-3.
82. Novita, N.; Subarno; Lestari N.S.; Anshari, G.Z.; Lugina, M.; Yeo, S.; Malik, A.; Asyhari, A.; Putra, C.A.S.; Gangga, A. Natural Climate Solutions in Indonesia: Wetlands are the Key to Achieve Indonesia's National Climate Commitment. *Environmental Research Letters* **2022**, *17*(11), 114045, doi: 10.1088/1748-9326/ac9e0a.